

# MID-IR ENHANCED GALAXIES IN THE COMA & VIRGO CLUSTER: LENTICULARS WITH A HIGH STAR FORMATION RATE

L. RIGUCCINI<sup>1,2,3</sup>, P. TEMI<sup>3</sup>, A. AMBLARD<sup>2,3</sup>, M. FANELLI<sup>2,3</sup>, F. BRIGHENTI<sup>4</sup>

(Dated: Accepted 2015 July 7)  
*Draft version March 2, 2024*

## ABSTRACT

We explore the properties of early-type galaxies (ETGs), including ellipticals (E) and lenticulars (S0), in rich environments such as clusters of galaxies (Virgo and Coma). The  $L_{24}/L_K$  distribution of ETGs in both Virgo and Coma clusters shows that some S0s have a much larger  $L_{24}/L_K$  ratio (0.5 to  $\sim 2$  dex) than the bulk of the ETG population. This could be interpreted as an enhanced star formation rate in these lenticulars. We compare the optical colors of galaxies in these two clusters and investigate the nature of these sources with a large  $L_{24}/L_K$  ratio by looking at their spatial distribution within the cluster, by analyzing their optical spectra and by looking at their optical colors compared to late-types. We obtain 10 Coma and 3 Virgo early-type sources with larger  $L_{24}/L_K$  ratios than the bulk of their population. We call these sources Mid-Infrared Enhanced Galaxies (MIEGs). In Coma, they are mostly located in the South-West part of the cluster where a substructure is falling onto the main cluster. MIEGs present lower g-r color than the rest of the ETG sample, because of a blue continuum. We interpret the excess  $L_{24}/L_K$  ratio as evidence for an enhanced star-formation induced as a consequence of their infall into the main cluster.

*Subject headings:* galaxies : early-type, cluster, star-formation

## 1. INTRODUCTION

The stellar content of galaxies is known to vary drastically with the environment. Clusters of galaxies are places of prime interest to study galaxy evolution as they offer a diverse set of physical conditions: virialized regions, merging substructures, etc. To a further extend, clusters of galaxies, being at the nodes of the filamentary structures of the Universe, are the ideal locations to understand the process of matter accretion from the surrounding large-scale structures.

Early-type galaxies (ETGs), elliptical and lenticular galaxies, used to be seen as a “red and dead” population, bereft of star-formation (e.g., Kormendy & Djorgovski 1989). Recent studies have indicated that some ETGs show signs of a current star-formation activity (e.g., de Zeeuw et al. 2002; Young et al. 2009; Shapiro et al. 2010; Amblard et al. 2014). Different studies have highlighted differences in the ETG stellar population in dense cluster and in lower density environment (e.g., Bower et al. 1990; Renzini 2006), based on certain spectral line ratios in these galaxies. Caldwell et al. (1993) found similar evidence, arguing that a basic visual inspection of ETG spectra was already capable of distinguishing differences in the stellar populations of ETGs lying in distinct environments (looking at Balmer absorption and emission lines). In this paper, we choose to study ETGs in a dense environment, in two nearby galaxy clusters, that are at a different stage of their evolution, the Virgo and Coma clusters. From statistical analyses of the positions and velocities of individual galaxies or through X-ray maps, significant substructures have been identified in these clusters underlying the fact that they are not virialized yet (e.g. Fitchett & Webster 1987;

Geller & Beers 1982; Oegerle & Hill 2001; White et al. 1993; Briel et al. 2001; Arnaud et al. 2001; Böhringer et al. 1994; Binggeli et al. 1993).

At a distance of 16.5 Mpc (Mei et al. 2007), Virgo is the closest galaxy cluster and is known to have a complex morphology with several components (e.g. de Vaucouleurs 1961; Pierce & Tully 1988; Yasuda et al. 1997; Federspiel et al. 1998; Binggeli et al. 1987; Ftaclas et al. 1984; Yoon et al. 2012). In a simplified way, Virgo is composed of 3 main substructures (cluster A with M87, cluster B with M49 and a sub-cluster of cluster A with M86), 3 clouds further away from the main cluster (M, W and W’) and the southern extension. These substructures are interconnected and fall into one another. They are located in the far outskirts of the Virgo Cluster, outside of the virial radius. They represent a great environment to study cosmic filaments linked to the large scale structure feeding into the cluster.

The Coma Cluster, located at a distance of 99 Mpc, has a complex morphology given that it is undergoing a merger, with a bright subcluster located around the south-west (SW) part of the cluster center (Adami et al. 2005). The Coma cluster has two central galaxies with similar brightness, instead of a single dominant galaxy as often is the case in clusters, a sign that Coma has undergone at least a relatively recent major merger. Coma has more galaxies, is more concentrated and is more virialized than Virgo (e.g., Weinzirl et al. 2014; Pimbblet et al. 2014; Smith et al. 2012). Simionescu et al. (2013) showed that the ongoing merger in the SW direction affects the surface radio profile of the cluster in this direction and that the intracluster medium (ICM) temperature along the eastern arm is systematically lower than in the north-west (NW) and west (W) directions from the center of the cluster out to 50 arcmin (1.4 Mpc). Using data from the X-ray satellite *Suzaku* launched in 2005, they also detected a boost in the surface brightness distribution in the 0.7-7 keV band towards the SW direction, location of an ongoing merger. They detect a X-ray emission out to a larger radii in the SW direction (as far as  $\sim 2.5$  Mpc) than towards the other directions.

riguccini@baeri.org

<sup>1</sup> Observatório do Valongo, Universidade Federal do Rio de Janeiro, Ladeira do Pedro Antônio 43, Saúde, Rio de Janeiro, RJ 20080-090, Brazil (riguccini@astro.ufrj.br)

<sup>2</sup> NASA Ames Research Center, Moffett Field, CA, USA

<sup>3</sup> BAER Institute, Sonoma, CA, USA

<sup>4</sup> Astronomy Department, University of Bologna, Via Ranzani 1, 40127 Bologna, Italy

Simionescu et al. (2013) and Urban et al. (2011) have produced similar studies (primarily thermodynamical) in Coma and Virgo respectively, which give an opportunity to compare the evolution of the two clusters. They found a similar trend for the ICM temperature, which decreases with the radius, while the ICM metallicity shows a different behavior in the outskirts of the clusters. Urban et al. (2011) observed a peak in the metallicity radial distribution at the outskirts of the Virgo cluster ( $\simeq 0.4$  Mpc), whereas the metallicity of the Coma cluster mainly decreases with the radius (Simionescu et al. 2013). The motivation of this present paper is to draw a comparison of the different mid-infrared (mid-IR) properties of the ETG population of the Virgo and Coma clusters. The paper is organized as follows. In section 2 we describe the data used in this work for both the Virgo and the Coma clusters. In section 3 we highlight the bimodality in the  $L_{24}/L_K$  distributions between Virgo and Coma. Virgo and Coma ETGs, that shows signs of enhanced star-formation, are selected and described in section 4 and 5, analyses in section 6. Section 7 briefly summarized our results. Throughout this paper, we adopt the standard  $\Lambda$ CDM cosmology:  $\Omega_m = 0.3$ ,  $\Omega_\Lambda = 0.7$  and  $H_0 = 70 \text{ km s}^{-1} \text{ Mpc}^{-1}$ .

## 2. DATA

We base our work on early-type galaxies in the Virgo and Coma clusters, simultaneously detected at  $24\mu\text{m}$  with the MIPS instrument onboard *Spitzer*, and in the  $K_s$ -band with the 2 Micron All-Sky Survey (2MASS). Morphological classifications are based on the  $T$  parameter, obtained from the Hyperleda database<sup>5</sup> (Paturel et al. 2003). We distinguish ellipticals with  $-5 \leq T < -3$  from lenticulars for which  $-3 \leq T < 0$ .

### 2.1. Virgo sample

The Virgo sample was assembled by cross identification between the Virgo Cluster Catalog (VCC, Binggeli et al. 1985) and the Temi et al. (2009b) sample, resulting in the selection of 58 galaxies with both  $K_s$ -band and  $24\mu\text{m}$  emission. Eight additional galaxies from the catalog of Leipski et al. (2012) were added to produce our Virgo Cluster sample. The total sample contains 66 sources evenly split between ellipticals ( $N = 34$ ) and lenticulars ( $N = 32$ ). All Virgo galaxies have high quality  $K_s$ -band photometry from 2MASS.

Our dataset comprises photometry collected from a number of *Spitzer* observing programs and is not derived from a single large flux-limited sample. To assess how representative this sample is when compared to the entire Virgo Cluster ETG population, we matched our sample against the Virgo Cluster HST-ACS survey and also against the early-type galaxy component of the Virgo Cluster Catalog. The ACS Virgo Cluster Survey Côté et al. (2004) obtained high-resolution imaging in two bandpasses (F475W and F850LP) for 100 early-type cluster members.

Our sample contains 24 of 25 ETGs brighter than  $B_T \leq 12.0$  (96%), 41 of 48 brighter than 13.0 (85%) and 54 of 78 brighter than 14.0 (69%). Based on the classifications provided in the VCC, the Virgo Cluster contains approximately equal numbers of bright E and S0 systems, similar to the the distribution in our mid-IR selected sample. We conclude that our sample should be representative of the bright ETGs in the Virgo Cluster. In constructing the samples to be compared, we wish to include only those sources in which the mid-IR luminosity is

derived exclusively from dust irradiated by starlight. Mid-IR fluxes can be boosted by radiatively warmed dust in accretion tori around active supermassive black holes (SBMHs) in the galaxy core. This AGN-driven excess mid-IR luminosity can lead to an overestimate of the star formation rate of the host galaxy. To exclude galaxies contaminated by AGN-heated dust, we utilize a BPT diagram diagnostic (Baldwin et al. 1981) to identify likely AGNs. From the SDSS spectroscopic catalog, we found 30 counterparts for our 66 Virgo sources: 9 of the 30 sources are star-forming, one showed emission line ratios consistent with a LINER designation (NGC 4168) and 20 are unclassifiable. Additionally, we examined the literature for known Virgo AGNs, adding NGC 4486 (M87), NGC 4374 (M84) and NGC 4261 to the excluded list.

The final Virgo sample is composed of 30 elliptical galaxies and 32 lenticulars. Four systems were excluded as AGNs, all ellipticals, whose  $24\mu\text{m}$  emission is expected to be dominated by heating from the central source. In this context we note the results of Leipski et al. (2012) who examined low-level nuclear activity in Virgo Cluster early-type galaxies by measuring the 2D  $24\mu\text{m}$  light distribution in these systems. They found little evidence for strongly enhanced  $24\mu\text{m}$  emission from a central AGN and concluded that SMBHs are generally quiescent, a consequence of low gas accretion rates.

### 2.2. Coma sample

For the Coma Cluster, we utilize the work of Mahajan et al. (2010) to build our ETG sample. Mahajan et al. (2010) used a combination of MIPS  $24\mu\text{m}$  observations, SDSS photometry and spectra to investigate the star formation history of galaxies in the Coma supercluster. All their galaxies from the SDSS data in the Coma supercluster region are brighter than  $r \sim 17.77$ , the completeness limit of the SDSS spectroscopic galaxy catalog. Their  $24\mu\text{m}$  fluxes are obtained from archival data covering  $2 \times 2 \text{ deg}^2$  for Coma Cluster. Bai et al. (2006) derived a  $24\mu\text{m}$  luminosity function of Coma using the same data and estimated the 80% completeness limit of the sample to be 0.33 mJy. They construct a catalog of 197 sources with SDSS and  $24\mu\text{m}$  counterparts within  $\sim 2h^{-1} \text{ Mpc}$  of the centre of Coma that we use to build our sample. Among the 197 sources, 134 galaxies are classified as ETGs, 38 have a morphological index of a late-type galaxy ( $T > 0$ ) and 25 sources do not have a morphological parameter. 124 sources among the 134 ETGs have been observed by 2MASS in the  $K_s$ -band. Our final sample of 124 sources is composed of 49 ellipticals and 75 lenticulars.

Adopting the same approach as for the Virgo sample, we choose to exclude systems with a strong AGN signal from our Coma dataset. Among the 124 ETGs of our Coma sample, 14 are flagged as AGN by Mahajan et al. (2010) using BPT diagram diagnostics or the Miller et al. (2003) criteria (1 elliptical and 13 lenticulars). We note here the opposite trend than that observed in Virgo, where all of the flagged AGNs are classed as ellipticals. The final Coma sample is composed of 48 elliptical and 62 lenticular galaxies, when excluding 1 elliptical and 13 lenticulars classified as AGNs.

### 2.3. Completeness and selection effect of the samples

One of the main focus of this present work is a comparison between the ETGs in the Coma and Virgo clusters. Since the clusters differ in distance by a factor of 6, the observations, that we use, do not reach the same depth. To avoid being affected by biases, we discuss the limiting fluxes of

<sup>5</sup> <http://leda.univ-lyon1.fr/>

the two samples hereafter. The Coma catalog from Mahajan et al. (2010) is 80% complete down to  $F_{24\mu\text{m}} = 0.33$  mJy. Once we apply this completeness limit to our Coma selection (Mahajan et al. (2010) catalog contains galaxies below  $F_{24\mu\text{m}} = 0.33$  mJy), the sample is reduced to 95 non-AGN sources, distributed between 42 elliptical and 53 lenticular galaxies. The Coma 80% completeness flux at  $24\mu\text{m}$  corresponds to a  $24\mu\text{m}$  flux of 12 mJy at 16.5 Mpc (Virgo) and to a  $24\mu\text{m}$  luminosity of  $10^{40.7}$  erg.s $^{-1}$ . The Coma completeness in the 2MASS  $K_s$  and SDSS  $r$  band corresponds to depths at Virgo distance of  $K_s < 10.53$  [Vega] (i.e.  $F_{K_s} > 40.8$  mJy) and  $r < 12.9$  [AB] (i.e.  $F_r > 25.3$  mJy). Applying this cut (the  $24\mu\text{m}$  completeness being the most stringent), the final Virgo sample is composed of 25 non-AGN sources: 10 elliptical galaxies and 15 lenticulars. For the remainder of this paper we consider only sources down to the same depth.

### 3. THE $L_{24\mu\text{m}}/L_K$ DISTRIBUTION OF ETGS IN VIRGO AND COMA

A tight correlation between the  $24\mu\text{m}$  luminosity and the K-band luminosity is expected for ellipticals, as already described in the literature (e.g., Temi et al. 2007a, 2009b; Young et al. 2009). Both studies conclude that most of the  $24\mu\text{m}$  emission in elliptical galaxies is circumstellar in origin. Temi et al. (2009b) found a larger scatter in the  $24\mu\text{m}$  - K-band relation for S0 galaxies than for ellipticals. Some S0 galaxies from their sample have the same star-forming properties as ellipticals, i.e. almost no star-formation, but some S0 galaxies have a larger  $L_{24\mu\text{m}}/L_K$  ratio, which is interpreted as the signature of a subpopulation of younger stars by Temi et al. (2009b). Young et al. (2009) noticed a population of galaxies with an even larger  $L_{24\mu\text{m}}/L_K$  ratio than Temi et al. (2007b) and found that CO-rich ETGs have  $24\mu\text{m}$  flux densities up to 15 times larger than sources with a pure circumstellar  $24\mu\text{m}$  emission.

#### 3.1. Detection of a bimodality

We explored the  $24\mu\text{m}$ -K-band relation for ETGs in both Virgo (red) and Coma (blue) down to the same depth as illustrated in Fig. 1, which presents the  $L_{24\mu\text{m}}/L_K$  ratio as a function of the K-band luminosity. Open and filled circles represent Elliptical and Lenticular galaxies respectively. Green rectangles and triangles indicate sources with strong AGN in the Virgo and Coma cluster respectively, for the rest of the study they will be discarded from our sample.

The three black squares represent sources for which the  $24\mu\text{m}$  flux is not safely known, and will be discussed in the following subsection. Fig. 1 shows that most galaxies lie at a constant  $L_{24\mu\text{m}}/L_K$  ratio of about 30, which is the expected ratio for galaxies with a gas-poor interstellar medium (ISM). Elliptical galaxies are located toward the bottom of the plot as expected (Temi et al. 2009b), while S0s span a range of  $\sim 2$  orders of magnitude in  $L_{24\mu\text{m}}/L_K$ . A few galaxies, mostly S0s, have a much larger flux ratio, some possibly due to the presence of a strong AGN but some due to a stronger star formation rate. Some of these galaxies with a large  $L_{24\mu\text{m}}/L_K$  ratio and a weak AGN activity have a flux ratio comparable to late-type galaxies and will be investigated in the next sections.

The distribution of the  $L_{24\mu\text{m}}/L_K$  ratio for each cluster for non-AGN sources (right side panel of Fig. 1) shows that the ratio peaks at a value  $0.30 \pm 0.08$  dex larger for Coma than Virgo and that Coma flux ratio distribution is broader than Virgo. Such differences in the flux ratio distribution are not

expected between ETGs of two local clusters. The error on the offset between the two distributions has been derived from the errors on the peak location of Virgo and Coma. To estimate these errors, we generated 100 simulations of our Virgo and Coma catalog.

The distribution of Virgo simulations peaks on average at  $30.14 \pm 0.07$  (our sample peaks at 30.16). The distribution of Coma simulations peaks on average at  $30.46 \pm 0.03$  (our sample peaks at 30.46). These simulations allow us to confirm that our 25 source sample is still large enough to constrain the difference in the peak location with enough statistical significance, the smaller richness of Virgo cluster is therefore not a statistical issue.

Reasons for the  $L_{24\mu\text{m}}/L_K$  ratio difference for the two clusters will be explored and tested in the next section. It implies that ETGs in Coma have either a larger amount of circumstellar dust per stellar mass or that they have an additional amount of cold ISM dust. Testing these galaxies with observations at longer wavelength could allow to disentangle these 2 scenarios. Another explanation could be that there is some photometric errors in one of these or both sets which produce either an overestimation of  $24\mu\text{m}$  fluxes for Coma galaxies or an underestimation of its K-band fluxes.

#### 3.2. Validity of the datasets

The differences observed in the  $L_{24\mu\text{m}}/L_K$  distributions between Coma and Virgo could come from photometric errors, especially since the photometry was calculated by different teams for these 2 clusters. In this subsection, we check the validity of these datasets by comparing them with the literature and with the WISE  $22\mu\text{m}$  catalog.

##### 3.2.1. Comparison with Leipski et al. (2012)

We find a  $\sim 0.5$  dex difference between the  $L_{24\mu\text{m}}$  distribution of Virgo and Coma with Virgo peaking at a shorter  $L_{24\mu\text{m}}$  value, and a  $\sim 0.25$  dex difference for the  $L_K$  distributions. Virgo cluster proximity (16 Mpc) might make it hard to find the apertures that encapsulate the total flux of each galaxy. If the aperture is too small, fluxes might be underestimated. Furthermore larger apertures require to better estimate the background flux, since a small error in the background flux will have a huge impact on the estimated flux. Since the major difference between Virgo and Coma is coming from the  $24\mu\text{m}$ , we checked our  $24\mu\text{m}$  fluxes (Temi et al. 2009b) with values from the literature (Leipski et al. 2012). Temi et al. (2009b) and Leipski et al. (2012) have 51 sources in common, but only 43 of those are real detection at  $24\mu\text{m}$  in Leipski et al. (2012). The 8 other sources are only upper limits and were not used. Fig. 2 shows a tight correlation between the  $24\mu\text{m}$  fluxes from Temi et al. (2009b) on the x-axis and fluxes from Leipski et al. (2012) on the y-axis. Excluding 3 sources that show unrealistic flux estimates (NGC4365, NGC4621, NGC4649), a linear fit to these data returns a slope of  $(0.98 \pm 0.01)$  and a y-intercept of  $(1.85 \pm 0.79)$  mJy, showing that on average these flux estimates are identical.

These 3 outliers, marked with black squares on Fig. 1, are elliptical galaxies and their fluxes are not expected to be as high as estimated by Leipski et al. (2012). Bressan et al. (2007) looked at the IRS *Spitzer* spectroscopy of early-type galaxies. NGC4365 and NGC4621 are part of their sample and they found that these two galaxies show clear evidence for dust emission beyond  $8\mu\text{m}$  which could explain the difficulties encountered to determine their  $24\mu\text{m}$  fluxes.

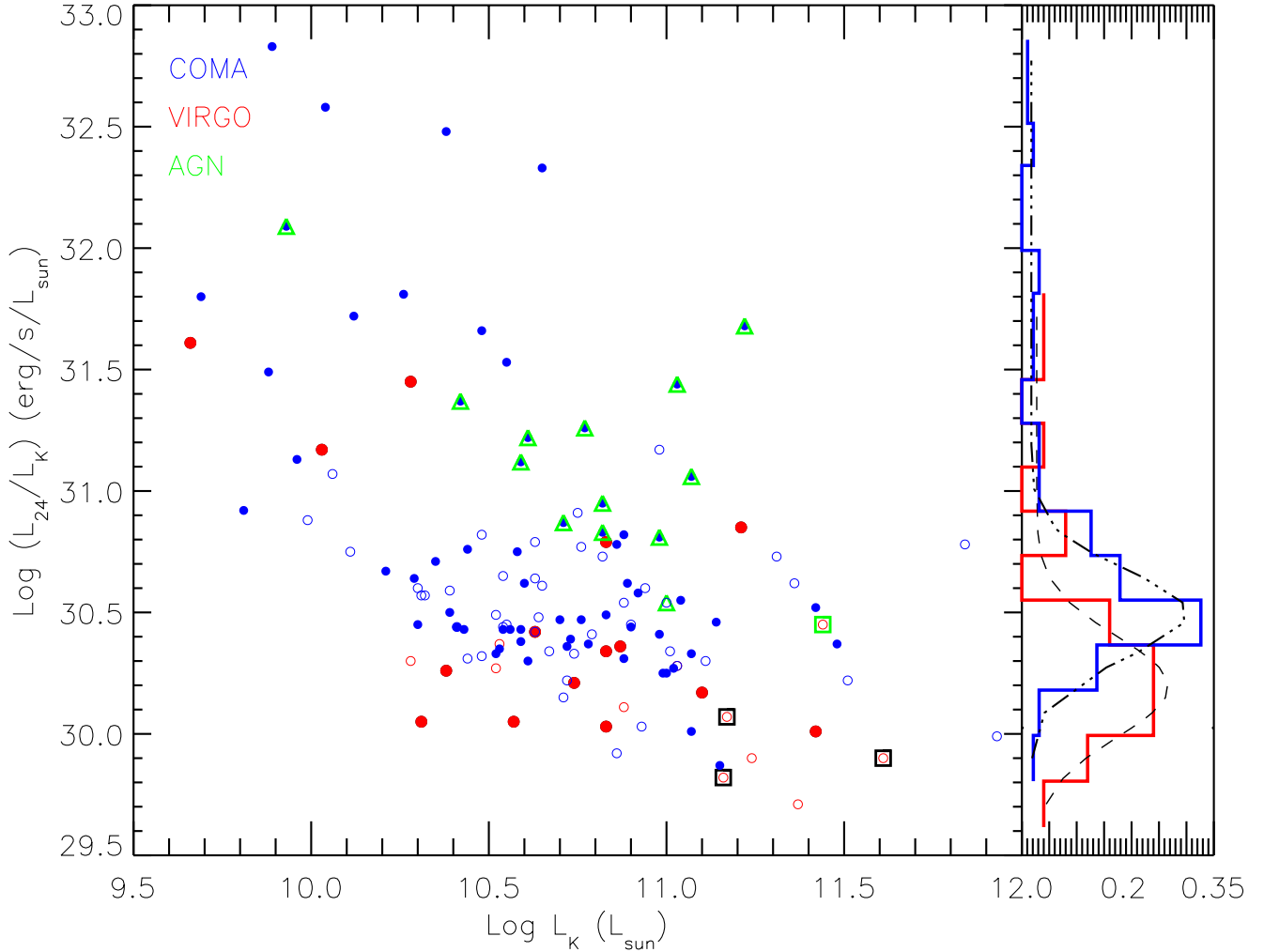


FIG. 1.—  $L_{24\mu\text{m}}/L_K$  distribution as a function of the K-band luminosity for our samples of early-type galaxies in Virgo (in red) and Coma (in blue). Elliptical galaxies are represented by open symbols while lenticulars are represented by filled ones. Known AGN sources are marked in green (green rectangles for Virgo and green triangles for Coma). The histograms on the right side show the  $L_{24\mu\text{m}}/L_K$  distribution for non-AGN sources. The black lines (dashed for Virgo and dotted-dashed for Coma) correspond to the best fit of each distribution. The 3 black rectangles are sources with extreme  $24\mu\text{m}$  fluxes according to Leipski et al. (2012) as detailed in Sect.3.2.1.

Martini et al. (2013) selected 38 ETGs to study their dust properties and they reported the  $24\mu\text{m}$  fluxes of NGC4365, NGC4621, NGC4649 to be respectively: 31.2 mJy, 33.2 mJy and 59.4 mJy. These values are closer to the fluxes obtained by Temi et al. (2009b) ( $22.2\pm4.7$  mJy,  $34.9\pm6.3$  mJy and  $108\pm10$  mJy respectively) than the ones obtained by Leipski et al. (2012) (110.01 mJy, 100.62 mJy and 342.10 mJy respectively). This figure shows evidence that our  $24\mu\text{m}$  fluxes are in agreement with another study and appear reliable.

### 3.2.2. Confirmation with WISE data

Although WISE does not provide the same sensitivity as *Spitzer*, WISE has mapped the entire sky and its  $22\mu\text{m}$  band (W4) is similar in wavelength range to *Spitzer*/MIPS  $24\mu\text{m}$  filter. The AllWISE catalogue (Wright et al. 2010; Mainzer et al. 2011) contains an aperture flux estimate for extended sources,  $w4\text{mag}$ , that has been used for instance by Davis et al. (2014). This catalog contains fluxes for both Virgo and Coma galaxies, that have been produced in the same fashion and should be less prone to systematic difference between the two clusters. 25 of our Virgo ETGs and 63 of our

Coma ETGs are detected at  $22\mu\text{m}$  by WISE down to 3.6 mJy, which corresponds to a magnitude of 8.4 [Vega] for Coma and 4.5 [Vega] for Virgo. Fig. 3 shows the distribution of the W4-K color for Virgo in red and Coma in blue. The two distributions are shifted with respect to each other by less than 1 dex in color, i.e. a  $\sim 0.37$  dex difference in luminosity, with Coma presenting a larger MIR/K ratio, as found previously with MIPS- $24\mu\text{m}$ . This reinforces our findings that Coma ETGs have, on average, a larger MIR-to-K luminosity ratio. A similar result is found even if we limit our analysis to the distributions of elliptical galaxies in the two clusters: a difference of  $\sim 0.35$  dex in the mean value of the two distribution is measured for ellipticals.

### 3.3. Tentative physical interpretations

Such a discrepancy can be ascribed to differences in the local environment, and the physical and dynamical conditions of the two clusters, as they have a profound effect on the galaxy population, the evolution and transformation of galaxies and their star formation history.

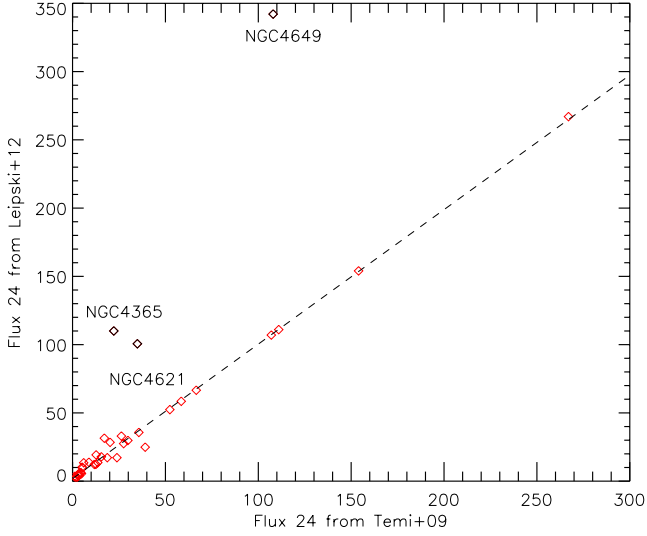


FIG. 2.— Correlation between the  $24\mu\text{m}$  flux estimates from (Leipski et al. 2012) and (Temi et al. 2009b). The dotted line is a fit obtained while excluding 4 outliers (red diamonds with names, except for NGC4472, since Leipski et al. (2012) estimate is much larger) and the dot-dashed lines are  $3\text{-}\sigma$  limits.

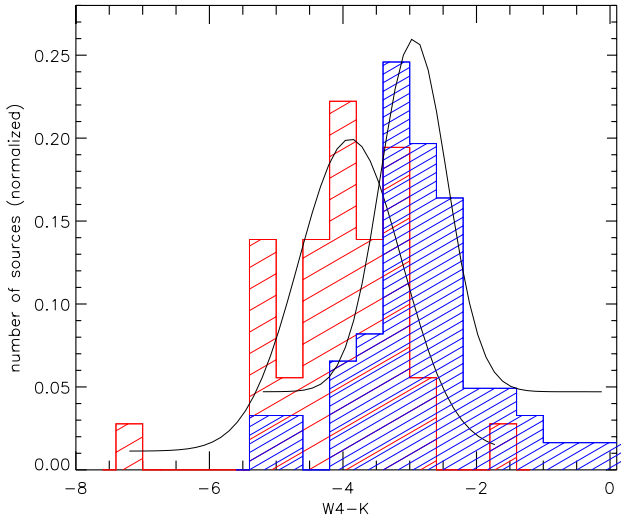


FIG. 3.— W4-K distribution for Virgo (red) and Coma (blue) with the best fit over plotted in black. W4 is the  $22\mu\text{m}$  channel of WISE.

Several channels of morphological transformation of disk galaxies into ETGs may be at play in cluster environment, including ram-pressure stripping of cold gas through interaction with the dense cluster medium (Abadi et al. 1999; Quilis et al. 2000; Smith et al. 2010), harassment (Farouki & Shapiro 1981; Moore et al. 1999) and gas consumption by star formation (Larson et al. 1980; Bekki et al. 2002). The interpretation of our data regarding the Coma cluster suggests that *pre-processing* due to environmental processes in small groups plays an important role in galaxy transformation and star formation activity before they enter the denser cluster environment. In a subsequent paper, we will investigate possible links between the morphological transformation and physical processes responsible for quenching the star formation in Virgo and Coma clusters. The discrepancy in the  $L_{24\mu\text{m}}/L_K$  ratio of the ETG distributions in the two clusters must be explained in relation to the physical properties of their environments.

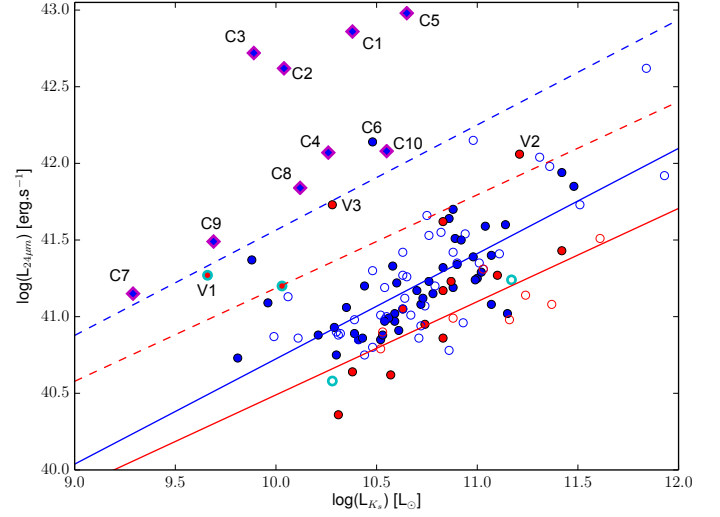


FIG. 4.—  $24\mu\text{m}$  luminosity as a function of the K-band luminosity in logarithmic scale for early-type galaxies in the Coma (in blue) and Virgo (in red) clusters. Magenta(cyan) diamonds represent star-forming sources in Coma(Virgo) as inferred with the BPT diagram diagnostic. The blue and red dashed lines represent the MIEG selection line for Coma and Virgo galaxies respectively, the solid lines represent the fitted  $\log(L_{24\mu\text{m}})\text{-}\log(L_K)$  relation.

Here we focus our attention on a sub-population of ETGs in Coma and Virgo by studying their star formation activity and by looking for radial trends and possible associations with infalling galaxy groups within the cluster. Recent studies of (optically) red-sequence galaxies in Coma (Smith et al. 2012; Rawle et al. 2013) have shown that the transformation of spirals into S0s is associated with cluster infall (Rawle et al. 2013) and that spatial trends in the ages of these galaxies are observed within the cluster (Smith et al. 2012; Rawle et al. 2013).

#### 4. MID-INFRARED ENHANCED GALAXIES (MIEGS): EXTREME SOURCES IN THE COMA & VIRGO CLUSTERS

##### 4.1. The Mid-Infrared Enhanced Galaxies (MIEGs) selection

Temi et al. (2009a,b) have shown that the K-band luminosity of elliptical galaxies correlates tightly with  $L_{24\mu\text{m}}$ . This correlation is approximately  $\log L_{24\mu\text{m}} \simeq \log L_K + 30.5$ , where  $L_{24\mu\text{m}}$  is expressed in  $\text{erg/s}$  and  $L_K$  in solar luminosity. Such a tight correlation is expected among elliptical galaxies since the  $8\text{-}24\mu\text{m}$  flux is produced by the collective emission from circumstellar dust flowing away from red giant stars. This mid-infrared emission has a de Vaucouleurs profile similar to optical starlight (Athey et al. 2002; Temi et al. 2008). When the  $\log(L_{24\mu\text{m}}/L_K)$  exceed the threshold of 30.5 it becomes a robust measurement of the specific star formation. We will focus our work on the most extreme sources, i.e. with the largest  $L_{24}/L_K$  ratio, in Fig. 1. They happen to be mostly lenticulars (filled symbols). Another way to look at the  $L_{24}/L_K$  relation is to plot the  $L_{24}$  luminosity as a function of  $L_K$  as illustrated on Fig. 4. We ran RANSAC (random sample consensus), an iterative fit method, on the Coma and Virgo data points to estimate a linear fit between the  $24\mu\text{m}$  and K band fluxes. After 50 iterative steps, the mean fitted relations are  $\log(L_{24\mu\text{m}}) = 0.69 \times \log(L_K) + 33.8$  for Coma and  $\log(L_{24\mu\text{m}}) = 0.61 \times$

TABLE 1  
COMA & VIRGO MID-INFRARED ENHANCED GALAXIES

Galaxy	Name	RA	Dec	cz	$r$	$M_r$	$(g-r)$
(1)	(2)	(3)	(4)	km sec <sup>-1</sup> (5)	(mag) (6)	(mag) (7)	(mag) (8)
C1	Mrk 57	194.6554	27.1762	7647	15.00	-20.24	0.36
C2	Mrk 56	194.6472	27.2649	7351	15.23	-19.92	0.28
C3	Mrk 53	194.0254	27.6781	4951	15.05	-19.23	0.34
C4	J12570456+2746228	194.2689	27.7730	7528	15.66	-19.55	0.66
C5	NGC 4926A	195.5328	27.6483	6889	14.36	-20.65	0.57
C6	J12581382+2810576	194.5575	28.1825	7169	14.71	-20.39	0.68
C7	J12575620+2734524	194.4843	27.5814	4943	16.08	-18.20	0.14
C8	J12583788+2727497	194.6577	27.4641	6287	15.69	-19.12	0.58
C9	J12582052+2725457	194.5855	27.4294	7562	16.78	-18.43	0.59
C10	J12584321+2854356	194.6800	28.9101	8353	14.96	-20.47	0.57
V1	NGC 4344	185.906	17.541	1058	12.46	-18.80	0.65
V2	NGC 4526	188.513	7.699	494	9.73	-21.41	0.86
V3	NGC 4694	192.063	10.984	1061	11.55	-19.75	0.41

NOTE. — Col. (1): Designation. Col. (2): Source name. Col. (3) & (4): J2000 epoch right ascension and declination as listed in NED. Col. (5): Recessional velocity, corrected to the local group centroid, as reported in NED. Col. (6): SDSS  $r$ -band Petrosian magnitude taken from the data release 8 and corrected for foreground extinction. Col. (7): Absolute  $r$ -band magnitude using the distances listed in Table 3 and 4. Col. (8):  $(g-r)$  color, corrected for foreground extinction.

$\log(L_K) + 34.4$  for Virgo (solid lines on Fig. 1).

With the goal to select sources lying well above the K- $24\mu\text{m}$  correlation, we select only sources above the upper  $5\text{-}\sigma$  line,

$$\begin{aligned} \log L_{24\mu\text{m}} &> 0.69 \times \log L_K + 34.7 \text{ for Coma,} \\ \log L_{24\mu\text{m}} &> 0.61 \times \log L_K + 35.1 \text{ for Virgo} \end{aligned} \quad (1)$$

These sources are defined as Mid-Infrared Enhanced Galaxies (MIEGs) and we will focus on these sources for the rest of this work. The Virgo MIEG selection line lies below Coma's one because its galaxies have a lower  $L_{24\mu\text{m}}/L_K$  on average, as described in the previous section. 10 Coma MIEG sources are lying above the Coma selection line (from C1 to C10), and 3 Virgo MIEG sources are lying above the Virgo selection line (from V1 to V3). These 13 MIEGs are all lenticulars. Fig. 4 shows the  $L_{24}$  distribution as a function of  $L_K$  for both Virgo (red) and Coma (blue) sources. The MIEG selection cut-offs (Eq. 1) are represented by dashed blue and red lines. Davis et al. (2014) fitted a similar relation between WISE  $22\mu\text{m}$  and 2MASS K-band for ATLAS<sup>3D</sup> ETGs that do not have a detection of CO molecular gas. Their best-fit ( $\log(L_{22\mu\text{m}}) = 1.00 \times \log(L_K) + 30.5$ ) is in good agreement with the  $L_{24}$ - $L_K$  relation for the bulk of the Coma and Virgo ETG population. Their results will be compared to our work in details in Sect. 6. The BPT diagnostic gives us informations on the nature of the ETG population: pink diamond (Coma) and light blue circles (Virgo) mark known star-forming sources. The large  $L_{24\mu\text{m}}/L_K$  value of these extreme sources can not be explained by AGN activity as 10 sources among the 13 MIEGs are known to be dominated by star-formation.

#### 4.2. Morphology of the Coma MIEGs

We focus on the 10 Coma galaxies lying above the  $2\text{-}\sigma$  line displayed in Fig. 4; these sources are labeled C1 through C10. Table 1 provides additional information on these 10 sources. To understand their morphological and photometric properties, we examined imagery from the SDSS and other archives. Three of the ten have been imaged with the Hubble Space Telescope (HST), permitting a higher resolution in-

spection. In Fig. 5 we present SDSS 3-color images of all 10; in Fig. 6, HST/ACS and HST/WFPC2 images in the F450W and F814W filters are used to produce RGB images of C1, C7 & C9.

##### 4.2.1. C1 - Mrk 57

C1 presents the most uncertain classification in this set. The SDSS image shows a disturbed blue disk with a likely tidal feature to the south. We note that Mrk 56, C2 in our list, is located  $\sim 5'$  to the north of C1, corresponding to a linear separation of  $\sim 150$  kpc at Coma with a  $\Delta V \sim 300$  km / sec. Both are distorted and actively forming stars. In the higher resolution HST image, C1 presents a more irregular morphology, with a prominent dust lane and blue knots. These images do not permit a clean classification for C1, which might be a disturbed late-type system or a gas-rich S0 undergoing a mild, interaction-induced starburst. We decide to keep C1 as part of our MIEG sample, but with a caution.

##### 4.2.2. C2 - Mrk 56

Similar in global color and luminosity to C1 & C3, C2 shows a distorted, diffuse, largely face-on disk, with a shell or tidal loop to the SW. The core appears elongated N-S with little evidence of a redder bulge. No substructure is obvious in the SDSS image.

##### 4.2.3. C3 - Mrk 53

The disk in C3 displays smoother outer isophotes compared to C1 & C2 with no prominent distortions and appears typical of "blue cloud" ETGs. In the center, there is a single, blue knot, offset  $\sim 3''$  S from the redder bulge and the hint of a dust patch to the west.

##### 4.2.4. C4

C4 shows an oval disk, a red bulge and globally smooth isophotes. A circumnuclear ring is likely present which is the source of the  $24\mu\text{m}$  emission.



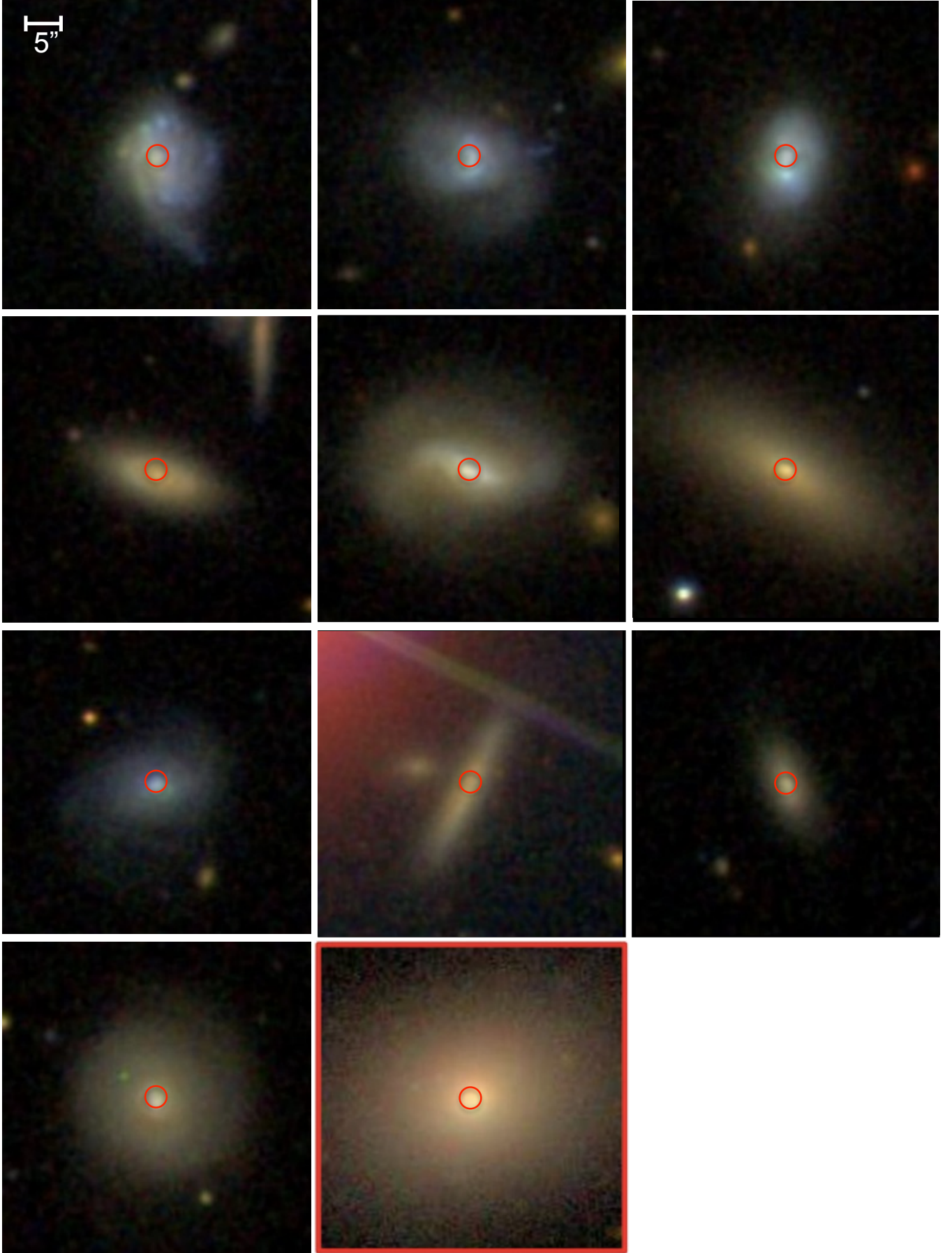


FIG. 5.—  $40'' \times 40''$  SDSS images of the MIEGs: first row from left to right: C1, C2, C3; second row from left to right: C4, C5, C6; third row from left to right: C7, C8, C9; fourth row from left to right: C10 and a typical ETG in Coma, framed in red. The SDSS fiber size ( $3''$  diameter) is represented at the center of the images as a red circle.

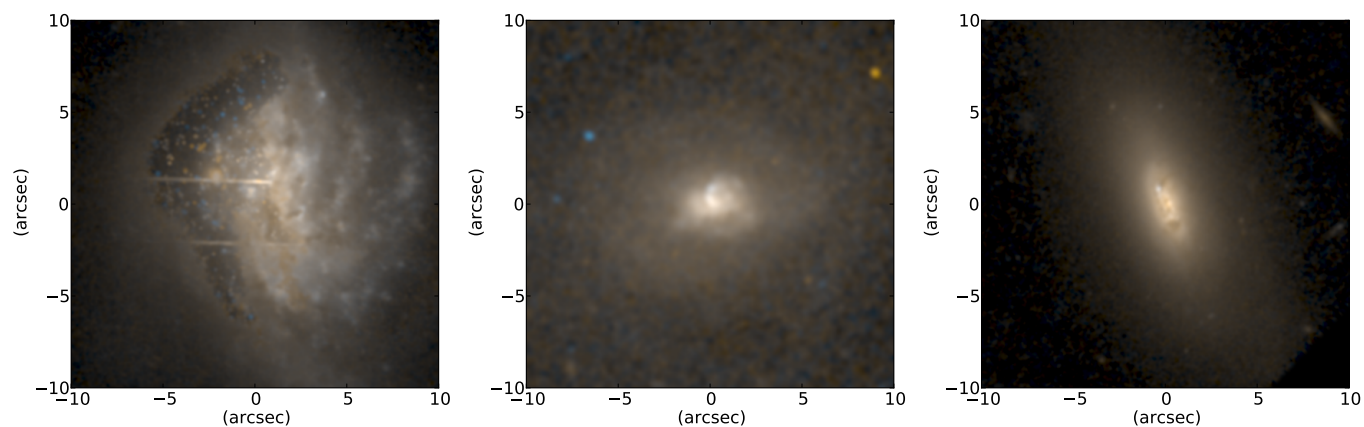


FIG. 6.— RGB images, produced with 2 HST filters, F814W and F450W, for some MIEGs: C1 (left), C7 (middle), C9 (right). The contrast of the intensity has been reduced by taking its value to the power of 0.4. All these MIEGs have a disturbed surface brightness, atypical for ETGs, with some blue knots and dust absorption structures.



#### 4.2.5. C5 - NGC 4926A

C5, the most optically luminous of the candidate MIEGs, contains a pear-shaped, diffuse outer disk in which a stellar bar extends from an elongated nuclear bulge at a PA  $\sim 70^\circ$ . The bar shows a distinct twist with radius. This system is also the brightest  $24\mu\text{m}$  source.

#### 4.2.6. C6

Similar to C4, this system displays smooth outer isophotes, an inclined, generally red disk with no structures evident in the SDSS image. The bulge is more prominent compared to C4, consistent with the 1.2 mag difference in absolute  $r$  magnitude between C4 & C6.

#### 4.2.7. C7

C7 has the oddest morphology in this sample. It is the bluest object, in (g-r), similar to C1-3, but about a factor of two less luminous. A prominent blue core is present within a somewhat irregular outer disk. The blue core and distorted disk are consistent with a global starburst, concentrated in the nucleus. The HST/WFPC2 image shows two intense blue knots in the core, each a few hundred parsecs across, embedded in an irregular patchy region about a kpc in diameter, which may be a circumnuclear ring. No spiral arcs or similar features are evident, suggesting that C7 is an ETG, despite the large formal uncertainty on its assigned  $T$  value. Caldwell et al. (1993, 1999) included C7 in a list of early type galaxies with enhanced star formation in the Coma infall region, designating it as an S0 but also quoting the Sa classification from Dressler (1980).

#### 4.2.8. C8

C8 is a highly inclined disk system with a clear radial color gradient and no prominent bulge. Due to its observed orientation, a robust classification is challenging. The absence of blue knots or a central dust lane suggests that C8 is properly an S0+ (e.g., Kormendy & Bender 2012).

#### 4.2.9. C9

C9 exhibits a small, diffuse disk with a modest central bulge. It is the least luminous, in SDSS  $r$ , of the candidate MIEGs and is intermediate in (g-r) color between the blue systems and the redder C6 & C8. The HST/ACS image shows structure in the inner kpc, possibly a ring or dust lane; at larger radii the disk is azimuthally symmetric, validating the ETG designation.

#### 4.2.10. C10

C10 appears as a face-on S0 with a bright core and a smooth, slightly asymmetric disk. The central region is bluer than typical S0 bulges with a dust patch visible between PA  $160^\circ$  and  $190^\circ$ . The disk shows a lower surface brightness extension in the NW quadrant. Globally, C10 is a slightly less luminous and more symmetric version of C5.

### 4.3. Summary

The candidate MIEGs presented here exhibit diverse morphologies, ranging from globally blue, asymmetric systems to redder, more relaxed galaxies. Seven show resolved evidence for enhanced star formation in addition to the  $24\mu\text{m}$  flux. C6 & C8 appear as normal, quiescent early-type galaxies, although we note that C8 (but not C6) is a GALEX FUV

source. We note that the observed redshifts for C3 and C7 are somewhat lower than the Coma cluster mean redshift, but within the range for possible current and future cluster members, given the large velocity dispersion of the cluster. These two systems may be part of the structures currently infalling into Coma, from either the foreground or background. In section 5, we examine the location of these MIEGs within the Coma region to explore the origin of their enhanced mid-IR emission with respect to the cluster substructure and thermodynamics of the hot gas.

### 4.4. Morphology of the Virgo MIEGs

We focus on the 3 objects lying above or close to the  $2\text{-}\sigma$  line displayed in Fig. 4; these sources are labeled V1 through V3. Table 1 provides additional information on these 5 sources. To understand their morphological and photometric properties, we examined imagery from the Hubble, SDSS and other archives. In Fig. 7 we present SDSS 3-color images of all 3.

#### 4.4.1. V1 - NGC4344

NGC 4344 is a face-on S0 whose optical appearance is dominated by a prominent, broken ring of blue starburst knots. Patches of dust are visible also, possibly causing the gaps in the ring. At the adopted distance, this ring has a diameter of 1.7 kpc. No HST images are available for this system.

#### 4.4.2. V2 - NGC4526

The SDSS images show that NGC 4526 is an inclined S0 ( $i \sim 78^\circ$ ) with a smooth outer disk and a prominent bulge surrounded by a substantial dust disk. This structure is well-resolved in Hubble ACS images (Fig. 8 which show a complex, filamentary dust distribution, visible at all angles around the bulge. Both the multicolor Hubble images and integral field spectra from SAURON (Kuntschner:06) indicate the presence of ongoing high-mass star formation with this dust disk. Reprocessed UV light from these young stars powers the enhanced  $24\mu\text{m}$  emission.

#### 4.4.3. V3 - NGC4694

NGC 4694 is a highly-inclined S0 with a blue core and asymmetric dust patches visible in the SDSS images. The Hubble data shows a chaotic dust morphology, more similar to that seen in VCC 571 than the more symmetric disk-like feature seen in NGC 4476 and NGC 4344. Outer isophotes are smooth, providing little evidence that the stellar disk has been perturbed.

### 4.5. Conclusions on the Virgo -MIEGs

Blue knots are interspersed within each structure indicating that young stars are forming within these disks. We can conclude that the MIEG phenomenon in the Virgo systems arises from an excess amount of dust, which appears to be related to the stellar disk most but not all systems.

Mapping of the location of the Virgo MIEGs within the cluster shows no correlation with position or the ROSAT-derived hot gas distribution. This result is different than that found for Coma, suggesting that more than one process can enhance the dust emission in early-type galaxies.

## 5. ANALYSIS

### 5.1. Distribution of the MIEGs among the cluster

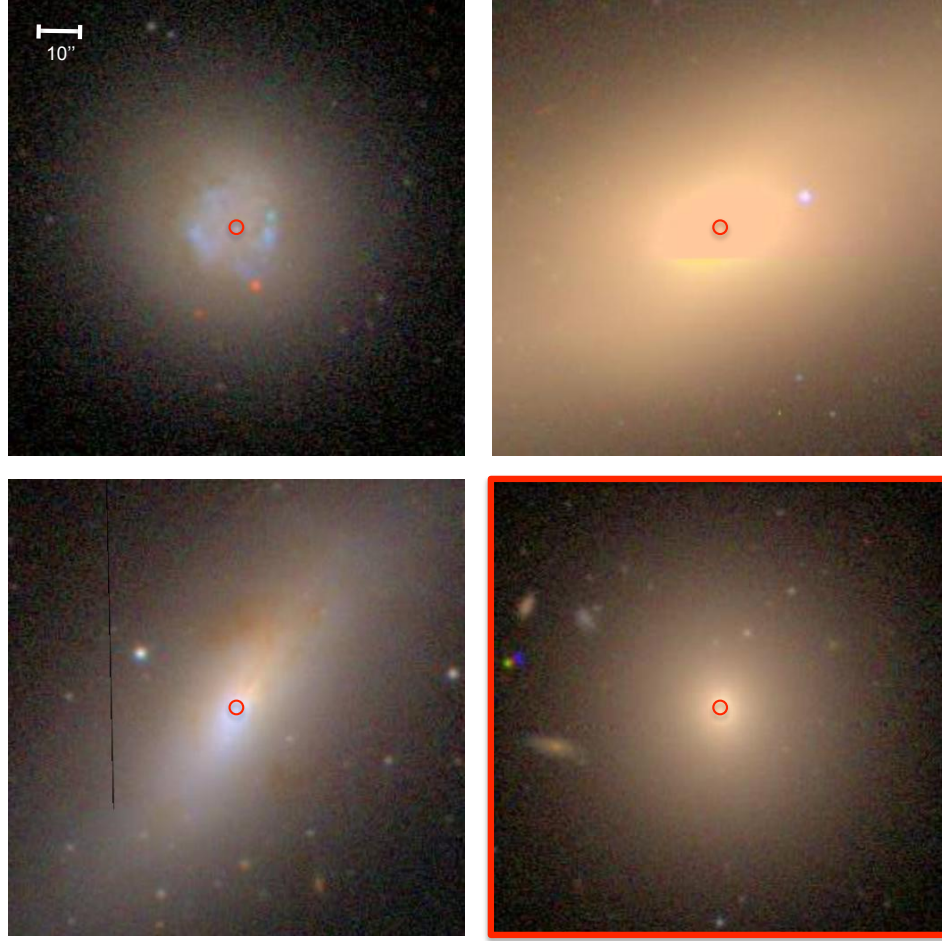


FIG. 7.—  $80'' \times 80''$  SDSS images of the MIEGs: first row from left to right: V1, V2; second row from left to right, V3 and a typical ETG in Virgo (framed in red). The SDSS fiber size ( $3''$  diameter) is represented at the center of the images as a red circle.

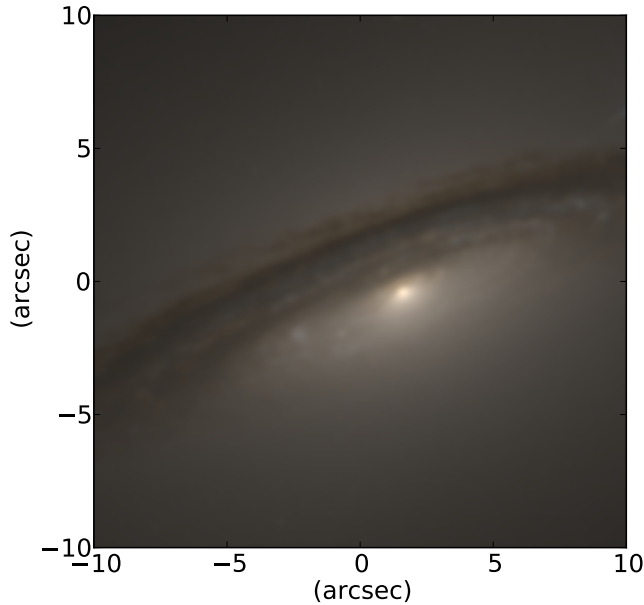


FIG. 8.— RGB image for the Virgo-MIEG V2, produced with 2 HST filters, among F475W, F555W, F850LP and F814W. The contrast of the intensity has been reduced by taking its value to the power of 0.4.

Fig. 9 shows the distribution of the ETGs in the Coma cluster with respect to their  $24\mu\text{m}/K$ -band luminosities ratio. Indeed, the circles are drawn proportionally to the  $L_{24}/L_K$  ratio of the sources. MIEGs are marked in orange on the figure. The ETGs are equally distributed between the core and the south region of the cluster ( $\sim 40\%$  of the sources from our Coma sample lie in each region) and only 20% of our sample lie in the north part of the cluster. In the core of the cluster, the whole ETGs population is non-MIEG i.e. does not show signs of star formation, while 20% of the ETGs are MIEGs in the southwest region (7 sources among the 10 MIEGs) against only 1% of the ETG sample being selected as MIEG in the north part of the cluster. The fact that the MIEGs are mainly located in outskirts of the galaxies and do not populate the core is expected since it is known that the star-forming galaxies preferentially avoid the core of the clusters and populate the outskirts (e.g., Kennicutt 1983; Dressler et al. 1999; Gallazzi et al. 2009). The exciting result here is that the MIEGs are not randomly distributed in the outskirts of the cluster but are mainly located in the southwest region of the Coma cluster, region known to experience an ongoing merger and a lot of thermodynamic activity. Briel et al. (1992); Watt et al. (1992) argue, from X-ray observations, that a gravitationally bound substructure may be falling into the Coma cluster. Neumann et al. (2001) showed, using X-ray data, that this southwestern substructure is in falling into the main cluster. Simionescu et al. (2013) show that this ongoing merger affects the surface

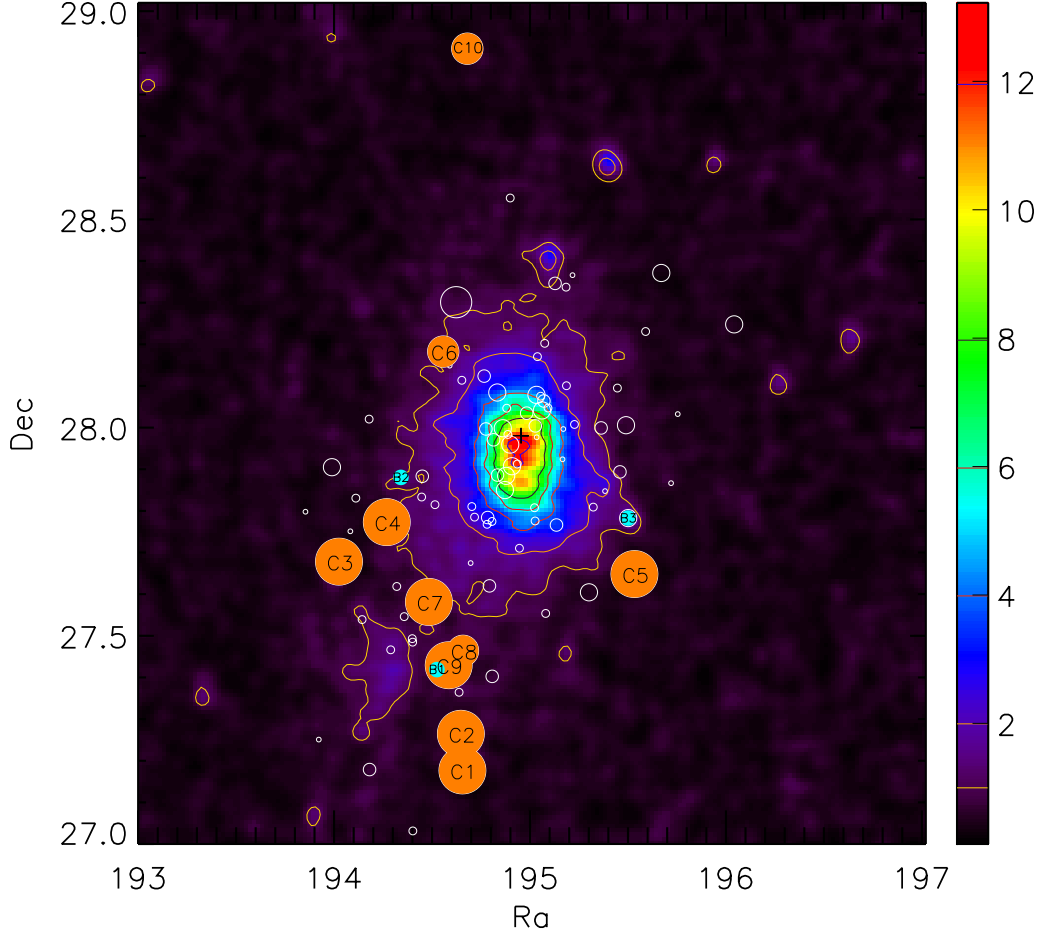


FIG. 9.— Distribution of the  $24\mu\text{m}$  detected sources (white open circles, orange and blue filled ones) on top of the ROSAT map of the Coma cluster. Orange filled circles represent the excess sources described in the text and populate mainly the southwest region of the cluster known to undergo a merger from an infalling substructure. The size of the circle is proportional to the ratio  $L_{24\mu\text{m}}/L_K$  (i.e. proportional to the specific star-formation rate of the source). The 6 blue sources are the “blue ETGs” that we define in sec. 5.2 and describe in sec. 5.2 & 5.3. The color bar on the right is the X-ray temperature in keV. The color of the filled circles are not linked to this color bar neither to the temperature.

radio profile of the cluster in this direction. Caldwell et al. (1993) found that galaxies with signs of star formation (strong Balmer-line absorption) are mainly located between the main part of the Coma cluster and the southwestern substructure, leading to the conclusion that the merger is triggering the star formation in these sources. Two scenarios have been proposed over the past decades and are still debated. One is in favor of infalling substructure triggering the star formation due to the increasing external pressure (e.g., Dressler & Gunn 1983; Evrard 1991; Abraham et al. 1996; Wang et al. 1997; Moss & Whittle 2000; Gavazzi et al. 2003; Poggianti et al. 2004). The second scenario invokes gas stripping in galaxies due to ram-pressure in the ICM that will quench the star-formation in galaxies during mergers (e.g., Tomita et al. 1996; Balogh et al. 1997, 1998; Fujita et al. 1999; Baldi et al. 2001). Our results on the MIEGs would be more in favor of the former effect and we argue that the infall of the substructure could enhance star-formation in some ETGs. Ferrari et al. (2005) found similar results in Abell 3921 from a *VRI* photometric and spectroscopic survey of the cluster. They argue that the ongoing merger in Abell 3921 has triggered a new star-formation episode in a non negligible fraction of their sample

of emission-line galaxies.

In the Virgo cluster, we observe the same expected trend where MIEGs are distributed mainly in the outskirts of the cluster, beyond the virial radius. Two of the three Virgo MIEGs (V1 & V3) are located at the border between cluster B and the W' cloud that is thought to infall onto the cluster B. Given the small number of MIEGs in Virgo and the large number of significant substructures in Virgo, it is hard to argue whether Virgo MIEGs support the idea that MIEGs are located in merging area or not. Virgo MIEGs seem at least to not be spatially distributed like normal ETGs, since most ETGs are within or in the proximity of the cluster A area, whereas most Virgo MIEGs are in the outskirts of the cluster.

### 5.2. Optical vs Infrared color color plot: comparison with late type

As discussed in the previous subsections, the extreme sources exhibit different properties than the rest of the ETG sample. The morphology of the MIEGs, described in sec. 4.2, confirm them as early-type sources. However their large  $L_{24}/L_K$  ratio encourage us to compare MIEGs to late-type galaxies to understand their evolutionary pathway. Fig. 10 dis-

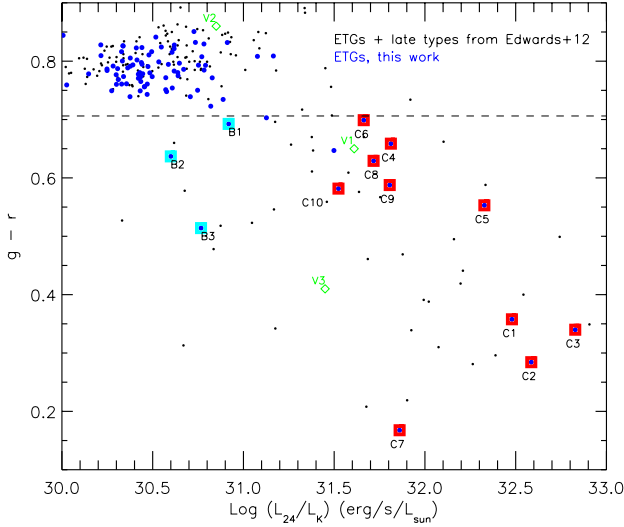


FIG. 10.— optical  $g-r$  color as a function of the  $24\mu\text{m}$ -to-K-band flux ratio for Coma sources: our Coma ETG sample (blue dots) with the excess sources marked in green (Virgo) and red (Coma) and the “blue ETGs” in cyan and compared to the galaxies (both early and late-type, black dots) from Edwards & Fadda (2011).

plays the optical ( $g-r$ ) color as a function of the  $24\mu\text{m}$ -to-K-band flux ratio of our  $24\mu\text{m}$ -detected ETG sample (blue dots) with the 13 MIEGs encircled in green and red and compared to late-type and early-types sources in Coma from Edwards & Fadda (2011). The general conclusion from these figures is that MIEGs clearly show a different behavior than normal ETGs as they are located at a different position in the color-color diagram. In Fig. 10, MIEGs have a lower ( $g-r$ ) color compared to the rest of the ETG sample, underlying a potential excess in the  $g$  band. Four MIEGs (C1, C2, C3 & C7) have far bluer colors than any other ETGs. Only late-type sources are as blue as these 4 MIEGs and with similar  $24\mu\text{m}$ -to-K-band flux ratios. V2, one of the Virgo MIEGs, is located with the bulk of ETGs way above the other MIEGs in terms of  $g-r$  colors, it is also the galaxy with the lowest  $L_{24\mu\text{m}}/L_K$  ratio and was barely above our selection line.

Three ETGs (marked as B1 to B3 on Fig. 10 and encircled in cyan) with  $F_{24}/F_K < 0.4$  (i.e. not MIEGs) have bluer color than the bulk of the ETGs, similar to the  $g-r$  colors of some MIEGs. These three sources are all lenticulars. The 3 “blue ETGs” seem to occupy areas of higher X-ray surface brightness and are located near a MIEG (looking at the distribution of the blue and orange sources on Fig. 9). They do not show sign of enhanced star-formation but present a bluer color than an ordinary early-type galaxy. Caldwell et al. (1993) have identified some ETGs in Coma with an abnormal spectrum mainly located in the SW field. They found that their abnormal-spectrum galaxies are slightly bluer (in B-V) than their normal counterparts. We found the same result but looking at the  $g-r$  color which is similar to the B-V used by Caldwell et al. (1993). We are providing evidence from the MIR photometry of likely the same phenomenon as Caldwell et al. (1993). These “blue” ETGs are therefore reliable candidates for being post-MIEG where the star-formation would have been quenched by ram pressure stripping by the ICM. Our “blue” galaxies are similar to the E+A galaxies from the literature (or more recently called “k+a” and “a+k” galaxies, e.g., Dressler & Gunn 1983; Franx 1993) who have undergone a recent star formation activity followed by a quiescent

phase. The southwest region of the Coma cluster is as an fine laboratory where we can observe transition-phase galaxies at different stages of their evolutionary path.

### 5.3. Analysis of the SDSS spectra

We obtain the SDSS spectra for 12 MIEGs (see Fig. 11 & 12, & 13). The  $3''$  fiber diameter (displayed as a red circle on Fig. 5 & 7) for the SDSS spectrograph (i.e.  $\sim 1.4$  kpc at Coma’s distance but only  $0.24$  kpc at Virgo’s distance) probes the central region of Coma MIEGs and a small inner fraction of that area for Virgo MIEGs. Given the smallness of the area probed, the interpretation of Virgo MIEG spectra has to be taken with caution, but is included here for completeness.

To compare with normal ETGs, we also obtained the SDSS spectra of a control sample, i.e. 10 ETGs in the Coma cluster that are not MIEGs. These spectra show globally the same features, i.e. no emission lines and a continuum increasing with wavelength. A typical ETG spectra is shown on Fig. 12 on the bottom-right panel (encircled in red) as an indication. C1, C2, C3, C5 & C7 present a similar spectrum with a rather blue continuum. This is confirmed by their  $g-r$  color on Fig. 10 where C1, C2, C3 & C7 exhibits bluer colors than any other ETGs from the sample ( $g-r < 0.35$ ). C5 also presents a rather blue  $g-r$  color ( $g-r \sim 0.55$ ) while the bulk of the ETG population (red points) lies at  $g-r \sim 0.8$ .

C4, C8, C9, C10, V1 has a flatter continuum and its  $g-r$  color is only slightly bluer than the bulk of the ETG.

C6 spectrum continuum is even more flat and resemble the one of a typical ETG.

All sources but C6 & V1 exhibit a spectrum with strong emission lines. Indeed, all the sources, but these 2, have a strong  $H_\alpha$  double emission lines, a  $\text{SII}$  emission line (around  $6800 \text{ \AA}$ ) and a  $H_\beta$  emission line, while C6 & V1 show a  $H_\beta$  absorption lines. C1, C2, C3, C5 & C7 have also a strong  $H_\gamma$  emission line and  $H_\delta$  is mostly seen as an absorption line except for C2. V1 lack of emission lines could be due to the smallness of SDSS beam, SDSS images show for instance that blue regions for V1 are located  $2.2''$  away from its center.

Three ETGs present  $g-r$  color as blue as some MIEGs (the ETGs encircled in cyan and marked as B1 to B3 on Fig. 10). Fig. 14 present the spectra of these 3 “blue ETGs”, it is significantly different from the MIEGs and more similar to “typical ETGs” with a slightly bluer continuum (and also quite similar to C6 & V1). This result supports the idea that the blue sources are on an advanced stage of the evolutionary path of the MIEGs and are therefore good post-MIEG candidate.

In Fig. 15, the equivalent widths of  $H_\alpha$  and  $H_\delta$  spectral emission lines are plotted as a function of the  $24\mu\text{m}/K$  flux ratio. The equivalent widths of the continuum-subtracted emission lines are obtained from the SDSS database and have been computed from straight integration over the corresponding bandpasses (emission is negative). Stellar absorption is taken into account.

A correlation is observed for both  $H_\alpha$  and  $H_\delta$  spectral emission lines with respect to the  $F_{24}/F_K$  ratio when the ratio is larger than about 0.8. At low  $F_{24}/F_K$ , no correlation with  $H_\alpha$  and  $H_\delta$  is observed for normal Coma ETGs (black dots), including the “blue” sources (black dots with a blue square). These two panels of Fig. 15 confirm the peculiarity of the MIEG spectra. The strong correlation at higher  $F_{24}/F_K$  can be explained by the fact that  $H_\alpha$  and  $H_\delta$  are indicators of star-formation activity, and such a correlation between  $F_{24}/F_K$  and

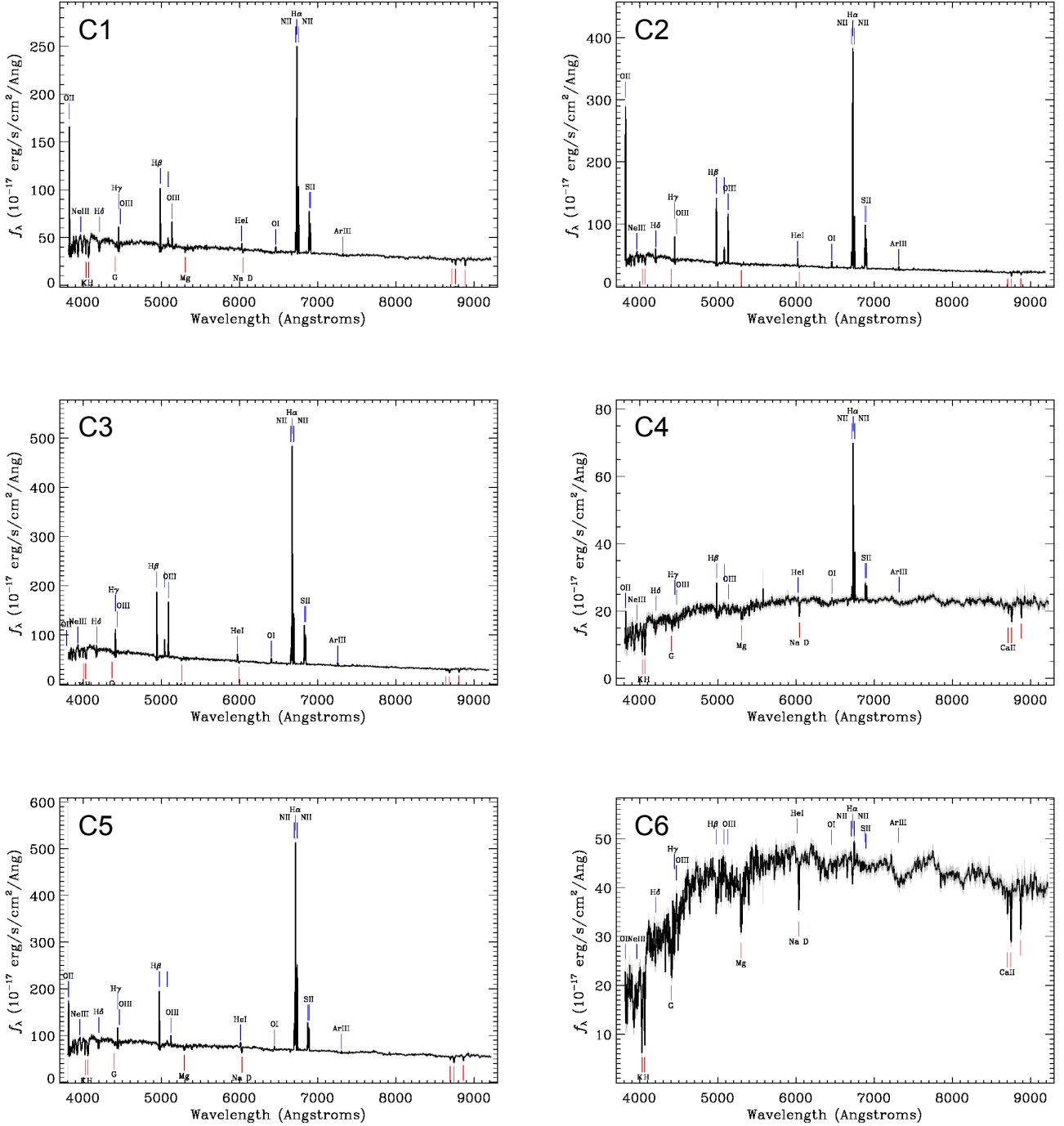


FIG. 11.— SDSS spectra of the first six Coma MIEGs (C1-C6).

the star-formation has already been observed by Temi et al. (2009b).

## 6. DISCUSSION

Galaxies with a large  $L_{24}/L_K$  ratio for ETGs, referred to as MIEGs, Mid-Infrared Enhanced Galaxies, are observed in both the Coma and Virgo clusters. In the Coma cluster, MIEGs are located primarily (70% of them) in the merging area of the central structure of the cluster and its main sub-

structure. In the Virgo cluster, the location of the MIEGs is more spread, but their spatial distribution do not follow the one of typical ETGs. Virgo MIEGs are predominantly (80% of them) located in the outskirts of the cluster, some in the vicinity of merging area, but it is not clear from their location if all MIEGs share the same origin. HST images, when available, show that MIEGs have disturbed but not identical morphologies, more images would be necessary to assess if morphologies indicate a common origin.



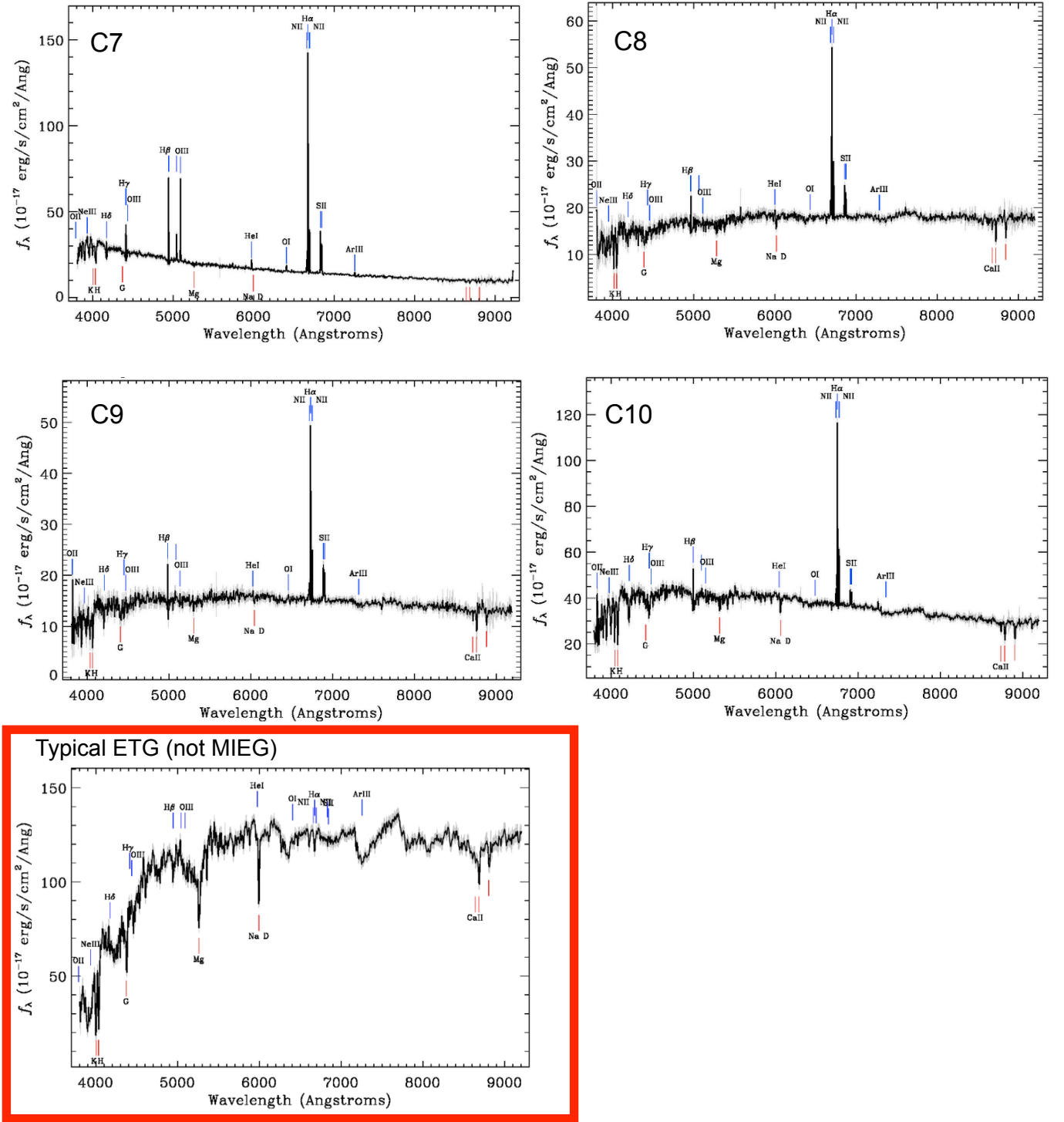


FIG. 12.— SDSS spectra of the last four Coma MIEGs (C7-C10). The last spectrum on the bottom left is a typical spectrum of an ETG in Coma which is not a MIEG (the spectrum corresponds to the source framed in red in Fig. 5).





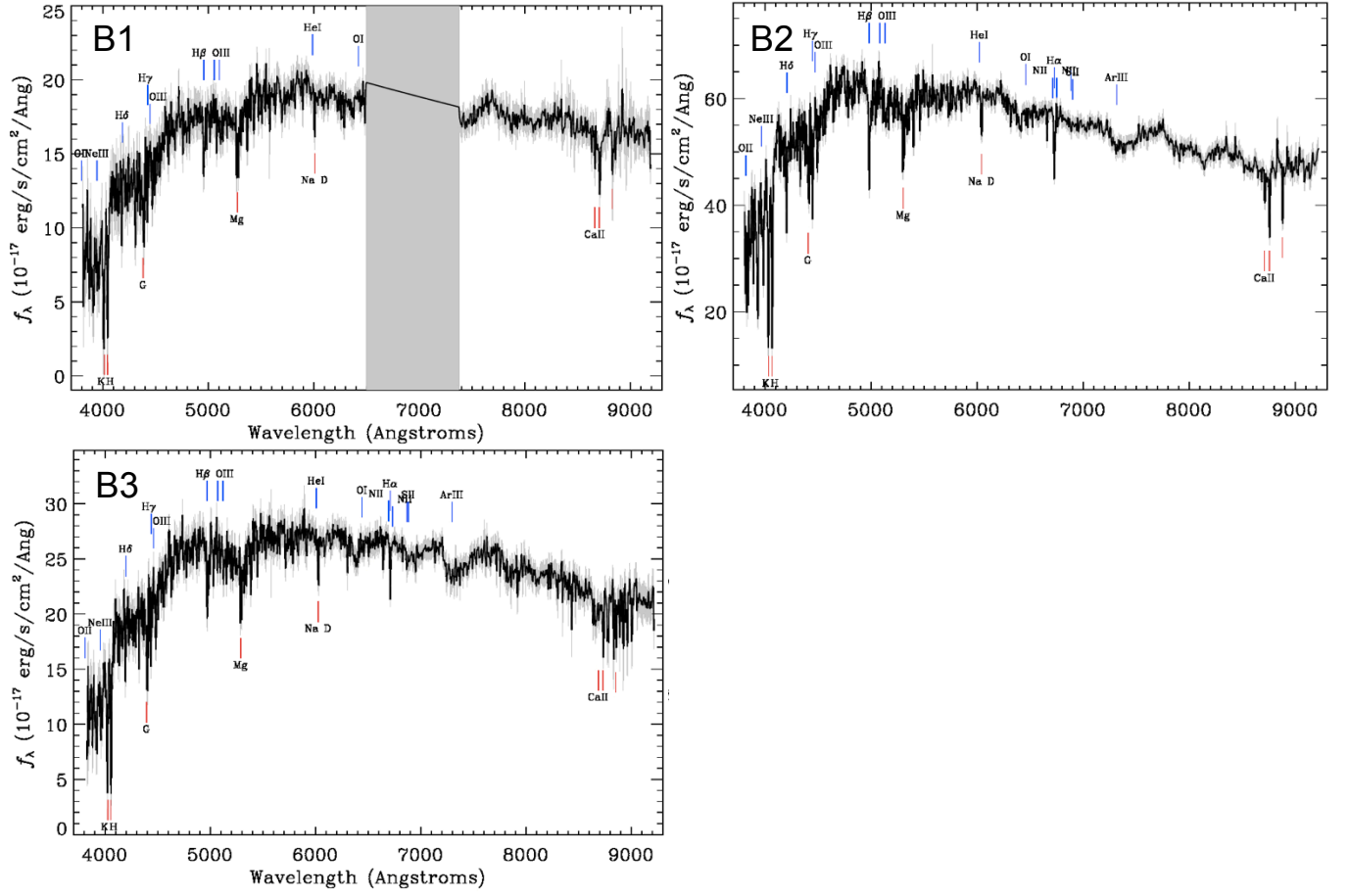


FIG. 14.— SDSS spectra of the 3 “blue ETGs” (noted B1 to B3 on Fig. 10).

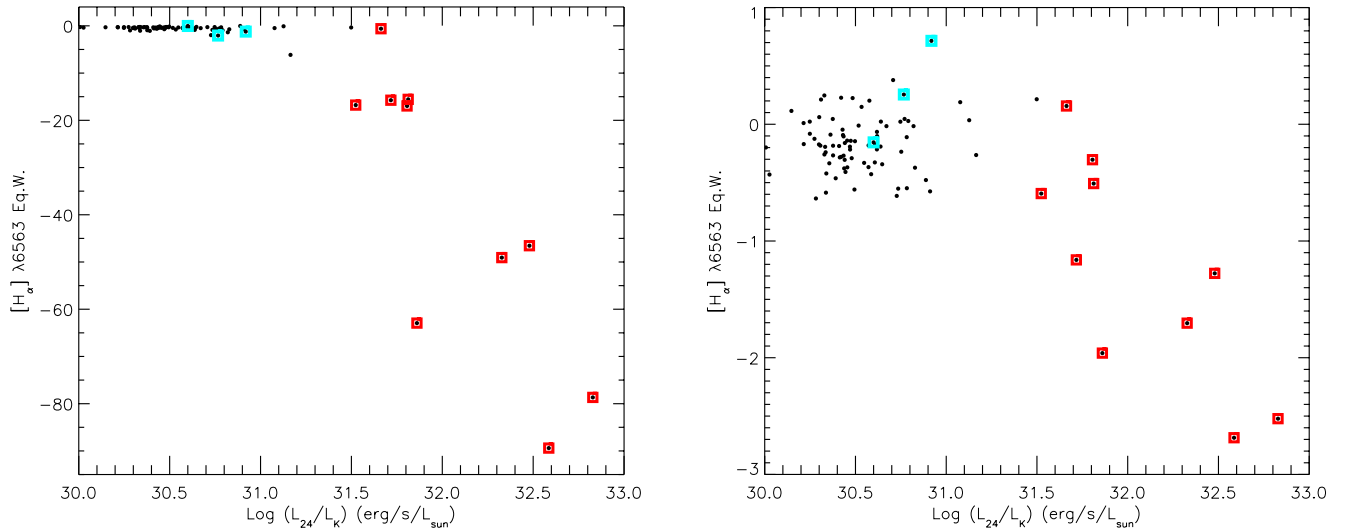


FIG. 15.— *Left*:  $[H_{\alpha}]\lambda 6563$  versus  $F_{24}/F_K$  for our Coma ETGs (emission is negative, absorption is positive). MIEGs are framed by red squares and “blue ETGs” are framed by blue squares. *Right*:  $[H_{\alpha}]\lambda 4102$  versus  $F_{24}/F_K$  for our Coma ETGs with the same color coding as the left panel.

vironments at a different stage of their evolution. We focus on the  $L_{24\mu m}/L_K$  distribution of the sources, a proxy for the star formation activity and we also obtain the optical colors, the detailed morphology and the optical spectra for a subset of our sample. Using these sets of data, we derived the following conclusions:

- The  $L_{24\mu m}/L_K$  distribution of ETGs in Coma peaks at a higher value than for Virgo ( $\sim 0.30 \pm 0.08$  dex difference).
- 13 ETGs with signs of strong star-formation activity (with a  $24 \mu m$  flux well above the expected value) are all lenticulars. We named them Mid-Infrared Enhanced Galaxies (MIEGs). MIEGs exhibit diverse morphologies, from globally, asymmetric systems to redder, more relaxed galaxies. The majority of the MIEGs in Coma (7 sources among the 10 ones) are located in the same neighborhood of the cluster, the south-west part of Coma, known for an ongoing merger activity. MIEGs also have bluer g-r color than the rest of the ETG population, with g-r colors similar to late-type galaxies. Their spectra are different from typical ETG spectrum, and feature strong emission lines (e.g.,  $H_\alpha$ ,  $H_\delta$ , OII) that are good indicators of star-formation. A tight correlation is also observed for the MIEGs between the  $H_\alpha$  and  $H_\delta$  emission lines equivalent widths and the  $F_{24\mu m}/F_K$  ratio, while “normal” ETGs do not show a correlation between their emission lines equivalent widths and their  $F_{24\mu m}/F_K$  ratio.
- Three ETGs in Coma present similar g-r colors than some of the MIEGs, they are bluer than the bulk of the ETG population because of their blue continuum. They do not show any strong emission lines that could account for star-formation activity like MIEGs. However these “blue sources” are all located in the neighborhood of MIEGs that hint toward a common history and a common evolution different from the rest of the ETG population.

These results emphasize the potential link between cluster merger activity and star-formation in galaxies. From a mid-to-near IR analysis, we have selected transiting galaxies at different stages of their evolutionary history. We have selected ETGs with signs of strong star formation and a subclass of ETGs with blue optical colors but no remaining of current star formation. MIEGs are a peculiar population of

lenticular galaxies with signs of enhanced star formation (high  $L_{24\mu m}/L_K$  ratios, strong emission lines, blue optical colors) potentially located in cluster substructure merging area. The known ongoing merger activity of the Coma region, where most of Coma MIEGs are located, could account for this enhancement. The hypothesis of cluster merging triggering the star formation has been widely discussed and accepted (e.g., Bekki 1999; Gavazzi et al. 2003; Poggianti et al. 2004), mostly for starbursts. In the other hand, the blue sources discussed in this work are good post-MIEG candidates where the recent star formation would have been quenched due to ram pressure stripping (e.g. Baldi et al. 2001). These blue sources would be the analogs of the post-starburst candidates in a evolutionary path for ETGs where MIEGs would be the analog of starburst galaxies. We will focus in the near future on the formation of these MIEGs, analyzing for instance their stellar population and looking for a second burst of star formation.

This work is based on archival data obtained with the Spitzer Space Telescope, which is operated by the Jet Propulsion Laboratory, California Institute of Technology under a contract with NASA. Support for this work was provided by NASA. This publication makes use of data products from the Two Micron All Sky Survey, which is a joint project of the University of Massachusetts and the Infrared Processing and Analysis Center/California Institute of Technology, funded by the National Aeronautics and Space Administration and the National Science Foundation. This publication makes use of data from SDSS-III. Funding for SDSS-III has been provided by the Alfred P. Sloan Foundation, the Participating Institutions, the National Science Foundation, and the U.S. Department of Energy Office of Science. The SDSS-III web site is <http://www.sdss3.org/>. SDSS-III is managed by the Astrophysical Research Consortium for the Participating Institutions of the SDSS-III Collaboration including the University of Arizona, the Brazilian Participation Group, Brookhaven National Laboratory, University of Cambridge, Carnegie Mellon University, University of Florida, the French Participation Group, the German Participation Group, Harvard University, the Instituto de Astrofísica de Canarias, the Michigan State/Notre Dame/JINA Participation Group, Johns Hopkins University, Lawrence Berkeley National Laboratory, Max Planck Institute for Astrophysics, Max Planck Institute for Extraterrestrial Physics, New Mexico State University, New York University, Ohio State University, Pennsylvania State University, University of Portsmouth, Princeton University, the Spanish Participation Group, University of Tokyo, University of Utah, Vanderbilt University, University of Virginia, University of Washington, and Yale University.

## APPENDIX

TABLE 2  
EARLY TYPE SAMPLE FOR THE VIRGO CLUSTER

Name	VCC	Dist	T	$F_{24\mu m}$	$\Delta F_{24\mu m}$	$K_s$	$\Delta K_s$	AGN	$\log L_{24\mu m}$	$\log L_{K_s}$	W4	$\Delta W4$
(1)	(2)	(Mpc)	(4)	(mJy)	(mJy)	(Vega mag)	(8)	(9)	( $\text{erg s}^{-1}$ )	( $L_\odot$ )	(Vega mag)	(13)
IC0798	VCC1440	7.70	-5.0	0.60	0.20	11.64	0.0750	0	38.72	8.46	10.29	2.01
IC3328	VCC0856	15.70	-5.0	0.45	0.080	11.30	0.123	0	39.22	9.22	9.59	1.16
IC3381	VCC1087	10.90	-4.1	0.52	0.100	11.05	0.119	0	38.96	9.00	...	...
IC3468	VCC1422	19.60	-4.9	0.16	0.080	10.51	0.113	0	38.96	9.73	...	...
IC3501	VCC1528	24.80	-3.5	0.24	0.080	11.24	0.0570	0	39.34	9.64	10.89	2.36
IC3602	VCC1743	31.40	-5.0	0.69	0.11	11.84	0.0780	0	40.01	9.61	7.88	0.22
IC3652	VCC1861	10.30	-4.9	0.22	0.080	11.05	0.127	0	38.54	8.96	10.13	1.72
IC3653	VCC1871	14.70	-5.0	0.77	0.12	10.58	0.0500	1	39.40	9.45	9.44	0.97
IC3773	VCC2048	16.70	-4.7	0.34	0.080	10.93	0.0700	0	39.15	9.42	9.96	1.78

TABLE 2 — *Continued*

Name	VCC	Dist (Mpc)	T	$F_{24\mu m}$ (mJy)	$\Delta F_{24\mu m}$ (mJy)	$K_s$ (Vega mag)	$\Delta K_s$	AGN	$\log L_{24\mu m}$ ( $\text{erg s}^{-1}$ )	$\log L_{K_s}$ ( $L_\odot$ )	W4 (Vega mag)	$\Delta W4$
(1)	(2)	(3)	(4)	(5)	(6)	(7)	(8)	(9)	(10)	(11)	(12)	(13)
NGC4168	VCC0049	33.70	-4.8	5.20	1.30	8.44	0.0210	2	40.95	11.03	6.97	0.38
NGC4261	VCC0345	31.60	-4.8	51.50	3.20	7.26	0.0280	2	41.89	11.44	...	...
NGC4267	VCC0369	15.90	-2.7	11.70	0.30	7.84	0.0230	0	40.65	10.62	6.62	0.37
NGC4344	VCC0655	17.90	-2.1	39.20	4.50	10.48	0.0240	1	41.27	9.66	...	...
NGC4350	VCC0685	15.90	-1.8	29.80	3.30	7.82	0.00800	0	41.05	10.63	5.92	0.14
NGC4352	VCC0698	31.00	-2.0	1.70	0.30	9.87	0.0450	1	40.39	10.38	8.01	0.57
NGC4365	VCC0731	17.10	-4.8	22.20	4.70	6.64	0.0290	0	40.98	11.16	5.33	0.20
NGC4371	VCC0759	14.30	-1.3	13.60	0.70	7.72	0.0230	0	40.62	10.57	6.10	0.23
NGC4374	VCC0763	18.40	-4.3	66.60	8.60	6.22	0.0230	2	41.53	11.39	4.66	0.14
NGC4377	VCC0778	21.30	-2.6	3.20	0.30	8.83	0.0160	0	40.33	10.47	5.93	0.12
NGC4379	VCC0784	14.20	-2.8	4.30	0.30	8.77	0.0180	0	40.11	10.15	7.84	0.53
NGC4382	VCC0798	18.50	-1.3	52.40	6.70	6.14	0.0210	0	41.43	11.42	...	...
NGC4406	VCC0881	17.10	-4.8	27.50	3.20	6.10	0.0280	0	41.08	11.37	4.99	0.22
NGC4417	VCC0944	15.90	-1.9	8.80	1.20	8.17	0.0280	0	40.52	10.48	6.40	0.21
NGC4421	VCC0966	23.10	-0.3	3.30	0.40	8.80	0.0210	0	40.42	10.56	...	...
NGC4434	VCC1025	26.80	-4.8	4.80	0.90	9.21	0.0290	0	40.71	10.52	8.06	0.47
NGC4435	VCC1030	15.90	-2.0	111.00	10.20	7.30	0.0160	0	41.62	10.83	4.68	0.12
NGC4442	VCC1062	8.70	-1.9	20.20	2.20	7.29	0.0240	0	40.36	10.31	5.62	0.13
NGC4458	VCC1146	17.20	-4.8	3.30	1.10	9.31	0.0220	0	40.16	10.09	8.52	0.96
NGC4459	VCC1154	16.10	-1.4	107.00	8.00	7.15	0.0110	0	41.62	10.90	4.44	0.072
NGC4464	VCC1178	15.90	-0.9	2.00	0.30	9.58	0.0280	0	39.88	9.92	9.16	0.78
NGC4472	VCC1226	17.10	-4.8	74.70	8.60	5.51	0.0170	0	41.51	11.61	4.10	0.15
NGC4473	VCC1231	15.70	-4.7	26.30	6.70	7.16	0.0230	0	40.99	10.88	5.70	0.19
NGC4474	VCC1242	15.90	-1.9	5.40	0.80	8.70	0.0150	0	40.31	10.27	7.12	0.30
NGC4476	VCC1250	17.20	-3.0	35.70	4.10	9.47	0.0200	1	41.20	10.03	6.03	0.064
NGC4477	VCC1253	17.10	-1.9	39.00	0.80	7.35	0.0130	0	41.23	10.87	5.53	0.17
NGC4478	VCC1279	18.10	-4.8	12.60	3.90	8.35	0.0130	0	40.79	10.52	6.72	0.27
NGC4479	VCC1283	15.90	-1.9	1.20	0.30	9.77	0.0300	1	39.66	9.84	8.59	0.79
NGC4482	VCC1261	27.80	-4.8	0.30	0.16	10.58	0.0810	1	39.54	10.00	12.11	10.00
NGC4483	VCC1303	13.70	-1.3	3.00	0.30	9.29	0.0320	1	39.92	9.91	8.05	0.64
NGC4486	VCC1316	16.10	-4.3	154.00	9.00	5.81	0.0190	2	41.77	11.44	3.78	0.069
NGC4489	VCC1321	17.90	-4.8	3.20	0.30	9.36	0.0280	1	40.18	10.11	8.27	0.54
NGC4515	VCC1475	15.90	-3.1	1.90	0.20	9.89	0.0230	1	39.86	9.80	8.39	0.38
NGC4526	VCC1535	16.90	-1.9	267.00	12.00	6.47	0.0200	0	42.06	11.21	...	...
NGC4528	VCC1537	20.80	-2.0	4.40	0.70	8.97	0.0220	0	40.45	10.40	7.58	0.56
NGC4552	VCC1632	15.30	-4.6	58.50	7.80	6.73	0.0240	0	41.31	11.03	5.12	0.14
NGC4564	VCC1664	15.00	-4.8	23.90	3.70	7.94	0.0210	0	40.90	10.53	6.58	0.38
NGC4570	VCC1692	25.90	-1.9	18.70	6.00	7.69	0.0130	0	41.27	11.10	6.04	0.35
NGC4578	VCC1720	18.50	-2.0	5.20	0.90	8.40	0.0330	0	40.43	10.52	6.55	0.40
NGC4612	VCC1883	26.60	-2.0	6.00	0.80	8.56	0.0260	0	40.80	10.77	6.93	0.32
NGC4621	VCC1903	18.30	-4.8	34.90	6.30	6.75	0.0260	1	41.24	11.17	5.45	0.23
NGC4623	VCC1913	26.60	-1.4	1.80	0.20	9.47	0.0370	0	40.28	10.41	6.93	0.32
NGC4636	VCC1939	17.10	-4.8	31.80	5.60	6.42	0.0350	0	41.14	11.24	4.83	0.23
NGC4638	VCC1938	21.70	-2.7	12.70	0.100	8.21	0.0190	0	40.95	10.74	7.04	0.68
NGC4649	VCC1978	17.10	-4.6	108.00	10.00	5.74	0.0210	0	41.67	11.52	3.14	0.047
NGC4660	VCC2000	12.80	-4.7	15.50	4.30	8.21	0.0170	1	40.58	10.28	6.43	0.17
NGC4694	VCC2066	18.20	-2.0	110.00	9.00	8.95	0.0290	0	41.73	10.28	4.64	0.039
NGC4754	VCC2092	16.80	-2.4	17.10	2.90	7.41	0.0300	0	40.86	10.83	5.82	0.22
NGC4762	VCC2095	15.90	-1.8	39.10	6.50	7.30	0.0290	0	41.17	10.83	...	...
NGC4262	VCC0355	15.40	-2.7	12.40	...	8.36	0.0160	0	40.64	10.38	...	...
VCC0571	VCC0571	23.80	-1.3	3.57	...	12.48	0.160	0	40.48	9.11	...	...
NGC4318	VCC0575	22.10	-5.0	5.87	...	10.35	0.0400	0	40.63	9.90	...	...
NGC4387	VCC0828	18.00	-4.9	5.64	...	9.15	0.0200	0	40.43	10.19	...	...
NGC4486B	VCC1297	16.30	-5.0	2.16	...	10.09	0.0170	1	39.93	9.74	...	...
NGC4486A	VCC1327	18.30	-5.0	6.06	...	9.01	0.0150	0	40.48	10.27	...	...
NGC4550	VCC1619	15.50	-2.1	9.80	...	8.69	0.0190	0	40.55	10.25	...	...
NGC4551	VCC1630	16.10	-4.9	5.91	...	8.87	0.0180	0	40.36	10.22	...	...

NOTE. — Col. (1): Name. Col. (2): Entry in the Virgo Cluster Catalog (Binggeli et al. 1985). Col. (3) Adopted distance. When available, values are taken from Tonry et al. (2001), otherwise they are from the NASA Extragalactic Database (NED) and corrected for  $H_0 = 70 \text{ km s}^{-1} \text{ Mpc}^{-1}$ . Col. (4): Morphological T parameter obtained from the Hyperleda database (Paturel et al. 2003). Col. (5) & (6): *Spitzer* MIPS  $24\mu m$  flux density and associated uncertainty from Temi et al. (2009b) for the 58 first sources, and from Leipski et al. (2012) for the last 8 sources. Col. (7) & (8):  $K_s$  magnitude and associated uncertainty, obtained from 2MASS. Col. (9): AGN classification flag, based partially on an optical BPT analysis. Unclassified source = 0, star forming galaxies = 1, AGN = 2. Col. (10): Log of the  $24\mu m$  luminosity. Here  $L_\lambda$  represents  $\lambda L_\lambda$  in  $\text{ergs s}^{-1}$ , as in Temi et al. (2009b). Col. (11): Log of the  $K_s$ -band luminosity in solar units. Col. (12) & (13): WISE  $22\mu m$  magnitude and associated uncertainty.

TABLE 3  
EARLY TYPE SAMPLE FOR THE COMA CLUSTER

RA J2000 (1)	Dec J2000 (2)	Dist Mpc (3)	T (4)	$F_{24\mu m}$ (mJy) (5)	$\Delta F_{24\mu m}$ (6)	$K_s$ (Vega mag) (7)	AGN (8)	$\log L_{24\mu m}$ $\text{erg s}^{-1}$ (9)	$\log L_{K_s}$ $L_\odot$ (10)	W4 (Vega mag) (11)	$\Delta W4$ (12)
194.475	28.500	106.6	-4.4	0.043	0.088	12.41	0	39.86	10.44	...	...

TABLE 3 — *Continued*

RA J2000 (1)	Dec J2000 (2)	Dist Mpc (3)	T (4)	$F_{24\mu\text{m}}$ (mJy) (5)	$\Delta F_{24\mu\text{m}}$ (6)	$K_s$ (Vega mag) (7)	AGN (8)	$\log L_{24\mu\text{m}}$ erg s <sup>-1</sup> (9)	$\log L_{K_s}$ $L_{\odot}$ (10)	W4 (Vega mag) (11)	$\Delta W4$ (12)
195.217	28.366	111.7	-3.1	1.389	0.099	10.82	0	41.41	11.11	9.38	0.88
194.899	28.551	110.9	-2.5	0.444	0.096	12.07	0	40.91	10.61	9.98	0.90
195.670	28.371	107.8	-0.2	2.885	0.143	11.33	0	41.70	10.88	9.04	0.63
195.536	28.387	110.8	-3.5	7.705	0.096	11.13	0	42.15	10.98	8.41	0.34
194.680	28.910	122.0	-2.0	5.350	0.090	12.42	1	42.08	10.55	8.90	0.41
193.922	27.251	103.5	-2.2	0.747	0.158	10.77	0	41.08	11.07	9.43	0.93
194.655	27.177	111.6	-1.2	39.096	0.323	12.65	1	42.86	10.38	6.47	0.06
194.638	27.364	101.7	-1.0	0.455	0.094	12.11	0	40.85	10.52	11.16	3.04
194.647	27.265	107.2	-1.8	24.348	0.101	13.43	1	42.62	10.04	...	...
194.025	27.678	71.9	-2.0	67.728	0.105	12.93	1	42.72	9.89	...	...
194.083	27.751	100.1	-5.0	0.576	0.102	11.57	0	40.94	10.72	10.00	0.93
194.269	27.773	109.9	-1.2	6.563	0.100	12.92	1	42.07	10.26	...	...
193.854	27.798	107.1	-3.6	1.201	0.469	10.94	0	41.31	11.03	8.63	0.46
194.111	27.831	91.4	-5.0	0.815	0.087	11.51	0	41.01	10.67	10.72	2.21
194.320	27.618	105.6	-4.1	0.424	0.078	12.46	0	40.85	10.41	...	...
194.717	27.785	82.4	-2.2	0.757	0.093	11.63	0	40.88	10.53	9.41	0.71
194.697	27.675	122.2	-2.1	0.470	0.367	10.93	0	41.02	11.15	...	...
194.324	27.811	103.0	-2.3	0.309	0.137	12.74	0	40.69	10.28	13.21	10.00
194.742	27.595	87.9	-2.5	0.200	0.096	12.05	0	40.36	10.42	12.90	10.00
194.781	27.768	92.0	-4.4	0.789	0.134	11.81	0	41.00	10.55	11.57	5.41
194.784	27.784	103.1	-4.9	2.207	0.139	11.09	0	41.54	10.94	...	...
194.647	27.596	111.8	-2.8	42.967	0.097	10.57	3	42.90	11.22	6.20	0.04
194.793	27.620	82.5	-4.1	0.771	0.098	12.15	0	40.89	10.32	10.17	1.10
194.946	27.710	122.9	-1.8	1.786	0.319	10.98	0	41.60	11.14	...	...
195.301	27.604	110.2	-2.5	0.635	0.096	12.70	0	41.06	10.35	...	...
195.474	27.624	114.9	-3.1	2.705	0.322	9.89	0	41.73	11.51	8.68	0.76
195.533	27.648	100.3	-1.9	63.709	0.098	11.74	1	42.98	10.65	5.84	0.03
194.806	27.775	99.6	-2.2	0.712	0.134	11.89	0	41.02	10.59	...	...
194.453	28.180	105.3	-5.0	0.312	0.098	11.74	0	40.71	10.70	...	...
194.375	28.188	100.8	-0.9	2.957	0.319	11.35	3	41.65	10.82	...	...
194.162	28.081	118.5	-2.5	0.268	0.087	13.19	0	40.75	10.22	...	...
194.558	28.183	104.5	-2.3	8.439	0.479	12.28	0	42.14	10.48	9.73	1.06
194.766	28.124	116.3	-4.6	4.750	0.326	10.29	0	41.98	11.36	8.26	0.30
194.590	28.149	114.6	-2.5	0.900	0.098	11.17	0	41.25	11.00	...	...
194.652	28.114	98.7	-2.4	1.452	0.094	11.27	0	41.32	10.83	8.73	0.52
194.881	28.047	101.5	-3.4	0.857	0.103	11.80	0	41.12	10.64	...	...
194.983	28.035	119.3	-2.6	1.813	0.148	11.16	0	41.59	11.04	10.20	1.44
194.861	27.999	97.1	-3.1	0.511	0.082	13.03	0	40.86	10.11	9.28	1.87
194.712	28.084	88.5	-2.3	0.270	0.095	12.48	0	40.50	10.25	9.76	0.84
194.833	28.084	68.0	-4.4	5.196	0.100	10.48	0	41.55	10.82	7.93	0.23
195.033	28.079	105.8	-4.8	2.033	0.097	11.59	0	41.53	10.76	9.87	0.90
195.027	28.004	105.8	-4.7	0.921	0.091	12.14	0	41.19	10.54	10.64	2.38
195.054	28.076	109.3	-3.3	0.570	0.100	12.26	0	41.01	10.52	9.42	0.81
195.071	28.064	89.3	-2.5	0.716	0.084	12.40	0	40.93	10.29	10.60	1.72
195.092	28.047	119.6	-2.4	0.729	0.098	11.55	0	41.19	10.88	9.74	1.05
195.186	28.101	96.1	-2.3	0.408	0.094	12.55	0	40.75	10.30	...	...
195.203	28.091	100.9	-4.2	2.282	0.094	10.90	3	41.54	11.00	9.30	0.63
195.038	28.170	98.6	-4.7	0.781	0.138	11.77	0	41.05	10.63	10.16	1.34
195.227	28.008	72.3	-4.6	2.903	0.333	10.41	0	41.35	10.90	9.29	1.03
195.061	28.041	83.2	-4.9	1.953	0.096	11.78	0	41.30	10.48	10.29	1.46
195.170	27.997	103.5	-4.6	0.452	0.101	11.66	0	40.86	10.71	10.20	1.30
195.363	27.999	111.5	-4.1	0.511	0.076	12.63	0	40.98	10.39	...	...
195.446	28.095	84.3	-2.8	1.137	0.101	11.20	0	41.08	10.72	...	...
195.490	28.006	113.1	-3.1	5.693	0.345	10.36	0	42.04	11.31	8.03	0.21
195.754	28.032	78.8	-1.9	2.114	0.080	10.31	0	41.29	11.02	8.28	0.25
195.736	28.070	113.0	-2.3	0.244	0.098	12.13	0	40.67	10.60	...	...
195.818	28.030	87.6	-0.5	9.402	0.321	11.15	3	42.03	10.77	7.24	0.12
195.937	28.084	81.2	-2.0	6.821	0.100	11.40	3	41.83	10.61	8.18	0.15
194.402	27.031	106.8	-0.2	0.774	0.132	11.69	0	41.12	10.73	...	...
194.300	27.103	105.8	-2.0	0.325	0.103	13.90	3	40.74	9.84	...	...
194.181	27.179	111.1	-3.0	4.747	0.352	10.04	0	41.94	11.42	9.02	0.81
194.289	27.466	108.7	-2.1	1.379	0.102	11.11	0	41.39	10.98	9.09	0.65
194.177	27.548	110.3	-2.0	0.243	0.144	13.89	0	40.64	9.88	...	...
194.399	27.493	106.9	-4.7	1.298	0.098	10.99	0	41.35	11.01	9.21	0.54
194.401	27.485	105.3	-4.7	0.576	0.094	12.14	0	40.98	10.54	9.56	0.71
194.295	27.405	90.2	-1.0	5.039	0.103	12.10	3	41.79	10.42	8.71	0.32
194.070	27.446	92.7	-4.0	0.236	0.095	12.12	0	40.48	10.43	10.00	0.93
194.358	27.546	79.3	-2.4	0.746	0.081	11.84	0	40.85	10.41	...	...
194.355	27.405	70.2	-2.5	14.344	0.099	12.78	2	42.02	9.93	...	...
194.484	27.581	71.7	-0.4	1.851	0.091	14.42	1	41.15	9.29	...	...
194.143	27.539	103.3	-4.4	0.743	0.120	11.60	0	41.07	10.74	10.52	1.61
194.525	27.419	83.3	-3.0	0.513	0.094	13.45	0	40.73	9.81	...	...
194.658	27.464	91.5	-2.5	5.507	0.104	12.88	1	41.84	10.12	...	...
194.586	27.429	110.4	-3.0	1.714	0.134	14.36	1	41.49	9.69	...	...
194.634	27.456	102.6	-2.5	0.497	0.104	12.44	0	40.89	10.39	11.08	4.23

TABLE 3 — *Continued*

RA J2000 (1)	Dec J2000 (2)	Dist Mpc (3)	T (4)	$F_{24\mu\text{m}}$ (mJy) (5)	$\Delta F_{24\mu\text{m}}$ (6)	$K_s$ (Vega mag) (7)	AGN (8)	$\log L_{24\mu\text{m}}$ erg s <sup>-1</sup> (9)	$\log L_{K_s}$ $L_{\odot}$ (10)	W4 (Vega mag) (11)	$\Delta W4$ (12)
195.080	27.554	85.6	-3.1	0.583	0.103	11.84	0	40.80	10.48	...	...
194.807	27.403	82.3	-1.9	1.650	0.084	11.44	0	41.22	10.60	9.85	0.95
193.989	27.905	95.2	-5.0	0.553	0.091	13.30	0	40.87	9.99	...	...
194.179	28.020	91.4	-1.9	1.764	0.335	10.92	0	41.34	10.90	9.38	0.68
194.341	27.880	108.1	-4.4	0.455	0.103	12.79	0	40.90	10.30	...	...
194.450	27.883	85.6	-4.7	1.665	0.103	11.40	0	41.26	10.65	10.64	2.78
194.447	27.833	88.8	-2.3	0.610	0.099	12.02	0	40.86	10.43	...	...
194.515	27.815	103.7	-2.3	0.575	0.102	11.98	0	40.97	10.59	11.84	7.52
194.591	27.968	87.4	-2.3	5.115	0.101	11.03	3	41.77	10.82	8.84	0.55
194.703	27.810	85.0	-2.2	1.586	0.095	11.12	0	41.23	10.76	10.00	1.36
194.814	27.971	69.2	-4.9	2.589	0.094	11.00	0	41.27	10.63	8.97	0.46
194.783	27.855	96.2	-2.2	2.779	0.103	11.50	3	41.58	10.71	9.48	0.80
194.769	27.911	93.4	-2.0	0.255	0.098	12.66	0	40.52	10.23	10.78	2.15
194.834	27.886	93.7	-3.4	0.583	0.099	12.46	0	40.88	10.31	10.35	1.53
194.750	27.968	121.5	-4.4	0.218	0.100	12.89	0	40.68	10.36	...	...
194.775	27.997	111.8	-2.1	1.739	0.098	11.38	0	41.51	10.89	9.52	0.97
194.733	27.833	110.3	-1.6	16.290	0.330	11.01	3	42.47	11.03	...	...
194.855	27.968	112.1	-3.3	0.217	0.094	12.61	0	40.61	10.40	12.10	7.51
194.908	27.907	117.3	-2.2	2.139	0.146	11.56	0	41.64	10.86	10.15	1.18
194.887	27.984	83.9	-2.1	1.395	0.098	11.25	0	41.17	10.70	9.48	0.76
194.935	27.913	97.0	-4.7	1.129	0.095	11.34	0	41.20	10.79	9.35	0.65
194.942	27.857	118.4	-3.3	0.152	0.096	12.04	0	40.50	10.68	...	...
194.899	27.959	104.4	-3.6	25.884	0.492	8.86	0	42.62	11.84	...	...
194.872	27.850	99.8	-4.2	3.066	0.152	11.50	0	41.66	10.75	...	...
194.878	27.884	68.8	-1.9	3.057	0.143	11.10	0	41.33	10.58	9.28	0.81
194.986	27.930	112.7	-2.3	0.228	0.080	12.62	0	40.64	10.40	...	...
195.166	27.924	109.5	-4.9	0.505	0.104	11.24	0	40.96	10.93	8.87	0.64
195.026	27.776	90.2	-3.3	0.464	0.104	12.04	0	40.75	10.44	10.22	1.35
195.023	27.808	95.8	-2.5	0.706	0.098	11.86	0	40.99	10.56	...	...
195.135	27.766	97.3	-1.5	0.538	0.099	12.78	0	40.88	10.21	9.26	0.55
195.034	27.977	94.3	-4.3	6.201	0.346	8.41	0	41.92	11.93	7.20	0.62
195.178	27.971	92.8	-1.9	4.849	0.099	10.76	3	41.79	10.98	8.22	0.33
195.323	27.809	106.7	-1.9	1.474	0.133	10.85	0	41.40	11.07	...	...
195.383	27.847	79.4	-3.1	0.638	0.345	10.72	0	40.78	10.86	...	...
195.633	27.936	96.4	-2.5	0.878	0.091	13.39	0	41.09	9.96	9.45	0.53
195.459	27.894	110.0	-4.2	1.446	0.096	11.37	0	41.42	10.88	10.35	1.54
195.501	27.783	102.8	-2.5	1.014	0.097	12.34	0	41.20	10.44	10.21	1.39
195.720	27.867	119.8	-0.6	0.816	0.098	11.28	0	41.24	10.99	11.75	5.51
194.623	28.301	85.3	-2.5	2.180	0.115	13.34	0	41.37	9.88	...	...
195.075	28.202	123.9	-2.1	3.111	0.492	10.14	0	41.85	11.48	7.81	0.23
195.128	28.346	87.2	-3.0	2.760	0.346	10.76	0	41.50	10.92	9.34	0.95
195.184	28.337	115.6	-2.3	0.709	0.145	11.74	0	41.15	10.78	...	...
194.758	28.225	116.9	-1.4	6.640	0.101	11.04	3	42.13	11.07	8.45	0.30
194.683	28.283	110.6	-2.5	0.052	0.098	13.76	0	39.98	9.93	...	...
195.543	28.192	83.2	-3.4	1.312	0.142	12.83	0	41.13	10.06	11.42	2.98
195.590	28.231	80.9	-1.9	0.949	0.144	11.57	0	40.97	10.54	9.40	0.89
195.590	28.256	99.0	-2.3	3.463	0.139	11.88	3	41.71	10.59	9.02	0.49
196.042	28.248	86.4	-3.1	2.378	0.099	11.47	0	41.42	10.63	10.81	1.64

NOTE. — Col. (1) & (2): J2000 epoch Right Ascension and Declination as listed in Mahajan et al. (2010). Col. (3) Adopted distance, converted from the redshift measurements from Mahajan et al. (2010), using  $H_0 = 70 \text{ km s}^{-1} \text{ Mpc}^{-1}$ . Col. (4): Morphological T parameter obtained from the Hyperleda database (Paturel et al. 2003). Col. (5) & (6): *Spitzer* MIPS  $24\mu\text{m}$  flux densities and associated uncertainties from Mahajan et al. (2010). The values in Col. (6) were provided to us by private communication from Mahajan. Col. (7):  $K_s$  magnitude from 2MASS. Col. (8): AGN classification from Mahajan et al. (2010): unclassified source are flagged as 0, 1 for star forming galaxies,  $\geq 2$  indicates an AGN. Col. (9): Log of the  $24\mu\text{m}$  luminosity. Col. (10): Log of the  $K_s$ -band luminosity in solar units. Col. (11) & (12): WISE  $22\mu\text{m}$  magnitude and associated error.

## REFERENCES

- Abadi, M. G., Moore, B., & Bower, R. G. 1999, MNRAS, 308, 947  
 Abraham, R. G., Smecker-Hane, T. A., Hutchings, J. B., Carlberg, R. G., Yee, H. K. C., Ellingson, E., Morris, S., Oke, J. B., & Rigler, M. 1996, ApJ, 471, 694  
 Adami, C., Biviano, A., Durret, F., & Mazure, A. 2005, A&A, 443, 17  
 Amblard, A., Riguccini, L., Temi, P., Im, S., Fanelli, M., & Serra, P. 2014, ApJ, 783, 135  
 Arnaud, M., Aghanim, N., Gastaud, R., Neumann, D. M., Lumb, D., Briel, U., Altieri, B., Ghizzardi, S., Mittaz, J., Sasseen, T. P., & Vestrand, W. T. 2001, A&A, 365, L67  
 Athey, A., Bregman, J., Bregman, J., Temi, P., & Sauvage, M. 2002, ApJ, 571, 272  
 Bai, L., Rieke, G. H., Rieke, M. J., Hinz, J. L., Kelly, D. M., & Blaylock, M. 2006, ApJ, 639, 827  
 Baldi, A., Bardelli, S., & Zucca, E. 2001, MNRAS, 324, 509  
 Baldwin, J. A., Phillips, M. M., & Terlevich, R. 1981, PASP, 93, 5  
 Balogh, M. L., Morris, S. L., Yee, H. K. C., Carlberg, R. G., & Ellingson, E. 1997, ApJ, 488, L75  
 Balogh, M. L., Schade, D., Morris, S. L., Yee, H. K. C., Carlberg, R. G., & Ellingson, E. 1998, ApJ, 504, L75  
 Bekki, K. 1999, ApJ, 510, L15  
 Bekki, K., Couch, W. J., & Shioya, Y. 2002, ApJ, 577, 651  
 Binggeli, B., Popescu, C. C., & Tammann, G. A. 1993, A&AS, 98, 275  
 Binggeli, B., Sandage, A., & Tammann, G. A. 1985, AJ, 90, 1681  
 Binggeli, B., Tammann, G. A., & Sandage, A. 1987, AJ, 94, 251  
 Böhringer, H., Briel, U. G., Schwarz, R. A., Voges, W., Hartner, G., & Trümper, J. 1994, Nature, 368, 828  
 Bower, R. G., Ellis, R. S., Rose, J. A., & Sharples, R. M. 1990, AJ, 99, 530



- Bressan, A., Panuzzo, P., Silva, L., Buson, L., Clemens, M., Granato, G. L., Rampazzo, R., Valdes, J. R., & Vega, O. 2007, in *Astronomical Society of the Pacific Conference Series*, Vol. 374, *From Stars to Galaxies: Building the Pieces to Build Up the Universe*, ed. A. Vallenari, R. Tantaló, L. Portinari, & A. Moretti, 333
- Briel, U. G., Henry, J. P., & Boehringer, H. 1992, *A&A*, 259, L31
- Briel, U. G., Henry, J. P., Lumb, D. H., Arnaud, M., Neumann, D., Aghanim, N., Gastaud, R., Mittaz, J. P. D., Sassee, T. P., & Vestrand, W. T. 2001, *A&A*, 365, L60
- Caldwell, N., Rose, J. A., & Dendy, K. 1999, *AJ*, 117, 140
- Caldwell, N., Rose, J. A., Sharples, R. M., Ellis, R. S., & Bower, R. G. 1993, *AJ*, 106, 473
- Côté, P., Blakeslee, J. P., Ferrarese, L., Jordán, A., Mei, S., Merritt, D., Milosavljević, M., Peng, E. W., Tonry, J. L., & West, M. J. 2004, *ApJS*, 153, 223
- Couch, W. J., & Sharples, R. M. 1987, *MNRAS*, 229, 423
- Davis, T. A., Young, L. M., Crocker, A. F., Bureau, M., Blitz, L., Alatalo, K., Emsellem, E., Naab, T., Bayet, E., Bois, M., Bournaud, F., Cappellari, M., Davies, R. L., de Zeeuw, P. T., Duc, P.-A., Khochfar, S., Krajnović, D., Kuntschner, H., McDermid, R. M., Morganti, R., Oosterloo, T., Sarzi, M., Scott, N., Serra, P., & Weijmans, A.-M. 2014, *ArXiv e-prints*
- de Vaucouleurs, G. 1961, *ApJS*, 42, 213
- de Zeeuw, P. T., Bureau, M., Emsellem, E., Bacon, R., Carollo, C. M., Copin, Y., Davies, R. L., Kuntschner, H., Miller, B. W., Monnet, G., Peletier, R. F., & Verolme, E. K. 2002, *MNRAS*, 329, 513
- Dressler, A. 1980, *ApJS*, 42, 565
- Dressler, A., & Gunn, J. E. 1983, *ApJ*, 270, 7
- Dressler, A., Smail, I., Poggianti, B. M., Butcher, H., Couch, W. J., Ellis, R. S., & Oemler, Jr., A. 1999, *ApJS*, 122, 51
- Edwards, L. O. V., & Fadda, D. 2011, *AJ*, 142, 148
- Evrard, A. E. 1991, *MNRAS*, 248, 8P
- Farouki, R., & Shapiro, S. L. 1981, *ApJ*, 243, 32
- Federspiel, M., Tammann, G. A., & Sandage, A. 1998, *ApJ*, 495, 115
- Ferrari, C., Arnaud, M., Ettori, S., Maurogordato, S., & Rho, J. 2006, *A&A*, 446, 417
- Ferrari, C., Benoist, C., Maurogordato, S., Cappi, A., & Slezak, E. 2005, *A&A*, 430, 19
- Fitchett, M., & Webster, R. 1987, *ApJ*, 317, 653
- Franx, M. 1993, *PASP*, 105, 1058
- Ftclas, C., Struble, M. F., & Fanelli, M. N. 1984, *ApJ*, 282, 19
- Fujita, Y., Takizawa, M., Nagashima, M., & Enoki, M. 1999, *PASJ*, 51, L1
- Gallazzi, A., Bell, E. F., Wolf, C., Gray, M. E., Papovich, C., Barden, M., Peng, C. Y., Meisenheimer, K., Heymans, C., van Kampen, E., Gilmour, R., Balogh, M., McIntosh, D. H., Bacon, D., Barazza, F. D., Böhm, A., Caldwell, J. A. R., Häußler, B., Jahnke, K., Jogee, S., Lane, K., Robaina, A. R., Sanchez, S. F., Taylor, A., Wisotzki, L., & Zheng, X. 2009, *ApJ*, 690, 1883
- Gavazzi, G., Cortese, L., Boselli, A., Iglesias-Paramo, J., Vilchez, J. M., & Carrasco, L. 2003, *ApJ*, 597, 210
- Geller, M. J., & Beers, T. C. 1982, *PASP*, 94, 421
- Kennicutt, Jr., R. C. 1983, *AJ*, 88, 483
- Kormendy, J., & Bender, R. 2012, *ApJS*, 198, 2
- Kormendy, J., & Djorgovski, S. 1989, *ARA&A*, 27, 235
- Larson, R. B., Tinsley, B. M., & Caldwell, C. N. 1980, *ApJ*, 237, 692
- Leipski, C., Gallo, E., Treu, T., Woo, J.-H., Miller, B. P., & Antonucci, R. 2012, *ApJ*, 744, 152
- Mahajan, S., Haines, C. P., & Raychaudhury, S. 2010, *MNRAS*, 404, 1745
- Mainzer, A., Bauer, J., Grav, T., Masiero, J., Cutri, R. M., Dailey, J., Eisenhardt, P., McMillan, R. S., Wright, E., Walker, R., Jedicke, R., Spahr, T., Tholen, D., Alles, R., Beck, R., Brandenburg, H., Conrow, T., Evans, T., Fowler, J., Jarrett, T., Marsh, K., Masci, F., McCallon, H., Wheelock, S., Wittman, M., Wyatt, P., DeBaun, E., Elliott, G., Elsbury, D., Gautier, IV, T., Gommillion, S., Leisawitz, D., Maleszewski, C., Micheli, M., & Wilkins, A. 2011, *ApJ*, 731, 53
- Martini, P., Dicken, D., & Storchi-Bergmann, T. 2013, *ApJ*, 766, 121
- Mei, S., Blakeslee, J. P., Côté, P., Tonry, J. L., West, M. J., Ferrarese, L., Jordán, A., Peng, E. W., Anthony, A., & Merritt, D. 2007, *ApJ*, 655, 144
- Miller, C. J., Nichol, R. C., Gómez, P. L., Hopkins, A. M., & Bernardi, M. 2003, *ApJ*, 597, 142
- Moore, B., Lake, G., Quinn, T., & Stadel, J. 1999, *MNRAS*, 304, 465
- Moss, C., & Whittle, M. 2000, *MNRAS*, 317, 667
- Neumann, D. M., Arnaud, M., Gastaud, R., Aghanim, N., Lumb, D., Briel, U. G., Vestrand, W. T., Stewart, G. C., Molendi, S., & Mittaz, J. P. D. 2001, *A&A*, 365, L74
- Oegerle, W. R., & Hill, J. M. 2001, *AJ*, 122, 2858
- Paturel, G., Petit, C., Prugniel, P., Theureau, G., Rousseau, J., Brouty, M., Dubois, P., & Cambrésy, L. 2003, *A&A*, 412, 45
- Pierce, M. J., & Tully, R. B. 1988, *ApJ*, 330, 579
- Pimblet, K. A., Penny, S. J., & Davies, R. L. 2014, *MNRAS*, 438, 3049
- Poggianti, B. M., Bridges, T. J., Komiyama, Y., Yagi, M., Carter, D., Mobasher, B., Okamura, S., & Kashikawa, N. 2004, *ApJ*, 601, 197
- Quilis, V., Ibáñez, J. M., & Sáez, D. 2000, *A&A*, 353, 435
- Rawle, T. D., Lucey, J. R., Smith, R. J., & Head, J. T. C. G. 2013, *MNRAS*, 433, 2667
- Renzini, A. 2006, *ARA&A*, 44, 141
- Serra, P., Oosterloo, T., Morganti, R., Alatalo, K., Blitz, L., Bois, M., Bournaud, F., Bureau, M., Cappellari, M., Crocker, A. F., Davies, R. L., Davis, T. A., de Zeeuw, P. T., Duc, P.-A., Emsellem, E., Khochfar, S., Krajnović, D., Kuntschner, H., Lablanche, P.-Y., McDermid, R. M., Naab, T., Sarzi, M., Scott, N., Trager, S. C., Weijmans, A.-M., & Young, L. M. 2012, *MNRAS*, 422, 1835
- Shapiro, K. L., Falcón-Barroso, J., van de Ven, G., de Zeeuw, P. T., Sarzi, M., Bacon, R., Bolatto, A., Cappellari, M., Croton, D., Davies, R. L., Emsellem, E., Fakhouri, O., Krajnović, D., Kuntschner, H., McDermid, R. M., Peletier, R. F., van den Bosch, R. C. E., & van der Wolk, G. 2010, *MNRAS*, 402, 2140
- Simionescu, A., Werner, N., Urban, O., Allen, S. W., Fabian, A. C., Mantz, A., Matsushita, K., Nulsen, P. E. J., Sanders, J. S., Sasaki, T., Sato, T., Takei, Y., & Walker, S. A. 2013, *ApJ*, 775, 4
- Smith, R. J., Lucey, J. R., Hammer, D., Hornschemeier, A. E., Carter, D., Hudson, M. J., Marzke, R. O., Mouhcine, M., Eftekharzadeh, S., James, P., Khosroshahi, H., Kourkchi, E., & Karick, A. 2010, *MNRAS*, 408, 1417
- Smith, R. J., Lucey, J. R., Price, J., Hudson, M. J., & Phillips, S. 2012, *MNRAS*, 419, 3167
- Temi, P., Brighenti, F., & Mathews, W. G. 2007a, *ApJ*, 660, 1215
- . 2007b, *ApJ*, 666, 222
- . 2008, *ApJ*, 672, 244
- . 2009a, *ApJ*, 695, 1
- . 2009b, *ApJ*, 707, 890
- Tomita, A., Nakamura, F. E., Takata, T., Nakanishi, K., Takeuchi, T., Ohta, K., & Yamada, T. 1996, *AJ*, 111, 42
- Tonry, J. L., Dressler, A., Blakeslee, J. P., Ajhar, E. A., Fletcher, A. B., Luppino, G. A., Metzger, M. R., & Moore, C. B. 2001, *ApJ*, 546, 681
- Urban, O., Werner, N., Simionescu, A., Allen, S. W., & Böhringer, H. 2011, *MNRAS*, 414, 2101
- Wang, Q. D., Ulmer, M. P., & Lavery, R. J. 1997, *MNRAS*, 288, 702
- Watt, M. P., Ponman, T. J., Bertram, D., Eyles, C. J., Skinner, G. K., & Willmore, A. P. 1992, *MNRAS*, 258, 738
- Weinzirl, T., Jogee, S., Neistein, E., Khochfar, S., Kormendy, J., Marinova, I., Hoyos, C., Balcells, M., den Brok, M., Hammer, D., Peletier, R. F., Kleijn, G. V., Carter, D., Goudfrooij, P., Lucey, J. R., Mobasher, B., Trentham, N., Erwin, P., & Puzia, T. 2014, *MNRAS*, 441, 3083
- White, S. D. M., Briel, U. G., & Henry, J. P. 1993, *MNRAS*, 261, L8
- Wright, E. L., Eisenhardt, P. R. M., Mainzer, A. K., Ressler, M. E., Cutri, R. M., Jarrett, T., Kirkpatrick, J. D., Padgett, D., McMillan, R. S., Skrutskie, M., Stanford, S. A., Cohen, M., Walker, R. G., Mather, J. C., Leisawitz, D., Gautier, III, T. N., McLean, I., Benford, D., Lonsdale, C. J., Blain, A., Mendez, B., Irace, W. R., Duval, V., Liu, F., Royer, D., Heinrichs, I., Howard, J., Shannon, M., Kendall, M., Walsh, A. L., Larsen, M., Cardon, J. G., Schick, S., Schwalm, M., Abid, M., Fabinsky, B., Naes, L., & Tsai, C.-W. 2010, *AJ*, 140, 1868
- Yasuda, N., Fukugita, M., & Okamura, S. 1997, *ApJS*, 108, 417
- Yoon, J. H., Putman, M. E., Thom, C., Chen, H.-W., & Bryan, G. L. 2012, *ApJ*, 754, 84
- Young, L. M., Bendo, G. J., & Lucero, D. M. 2009, *AJ*, 137, 3053